KOMPETENZZENTRUM WasserBerlin

REPORT

Cicerostr. 24
D-10709 Berlin
Germany
Tel +49 (0)30 536 53 800
Fax +49 (0)30 536 53 888
www.kompetenz-wasser.de

GIS approach to localize critical source areas of diffuse nitrate pollution

Case study on the Ic catchment, France

Project acronym: AQUISAFE 2

by

Anna Bugey
Department Surface Water
Kompetenzzentrum Wasser Berlin gGmbH

for

Kompetenzzentrum Wasser Berlin gGmbH

Preparation of this report was financed in part through funds provided by

VEOLIA WATER

Berlin, Germany
2010

Important Legal Notice

Disclaimer: The information in this publication was considered technically sound by the consensus of persons engaged in the development and approval of the document at the time it was developed. KWB disclaims liability to the full extent for any personal injury, property, or other damages of any nature whatsoever, whether special, indirect, consequential, or compensatory, directly or indirectly resulting from the publication, use of application, or reliance on this document. KWB disclaims and makes no guaranty or warranty, expressed or implied, as to the accuracy or completeness of any information published herein. It is expressly pointed out that the information and results given in this publication may be out of date due to subsequent modifications. In addition, KWB disclaims and makes no warranty that the information in this document will fulfill any of your particular purposes or needs. The disclaimer on hand neither seeks to restrict nor to exclude KWB's liability against all relevant national statutory provisions.

Wichtiger rechtlicher Hinweis

Haftungsausschluss: Die in dieser Publikation bereitgestellte Information wurde zum Zeitpunkt der Erstellung im Konsens mit den bei Entwicklung und Anfertigung des Dokumentes beteiligten Personen als technisch einwandfrei befunden. KWB schließt vollumfänglich die Haftung für jegliche Personen-, Sach- oder sonstige Schäden aus, ungeachtet ob diese speziell, indirekt, nachfolgend oder kompensatorisch, mittelbar oder unmittelbar sind oder direkt oder indirekt von dieser Publikation, einer Anwendung oder dem Vertrauen in dieses Dokument herrühren. KWB übernimmt keine Garantie und macht keine Zusicherungen ausdrücklicher oder stillschweigender Art bezüglich der Richtigkeit oder Vollständigkeit jeglicher Information hierin. Es wird ausdrücklich darauf hingewiesen, dass die in der Publikation gegebenen Informationen und Ergebnisse aufgrund nachfolgender Änderungen nicht mehr aktuell sein können. Weiterhin lehnt KWB die Haftung ab und übernimmt keine Garantie, dass die in diesem Dokument enthaltenen Informationen der Erfüllung Ihrer besonderen Zwecke oder Ansprüche dienlich sind. Mit der vorliegenden Haftungsausschlussklausel wird weder bezweckt, die Haftung der KWB entgegen den einschlägigen nationalen Rechtsvorschriften einzuschränken noch sie in Fällen auszuschließen, in denen ein Ausschluss nach diesen Rechtsvorschriften nicht möglich ist.

Colophon

Title

GIS approaches to localize critical source areas of diffuse nitrate pollution

Case study on the Ic catchment, France

Authors

Anna Bugey, Kompetenzzentrum Wasser Berlin gGmbH, Berlin, Germany

Quality Assurance

Andreas Matzinger, Kompetenzzentrum Wasser Berlin gGmbH, Berlin, Germany

Dagmar Orlikowski, Kompetenzzentrum Wasser Berlin gGmbH, Berlin, Germany

Emmanuel Soyeux, Veolia Environnement Recherche & Innovation (VERI), Paris, France

Christelle Pagotto, Veolia Water, Technical Direction, Saint-Maurice, France

Stefan Julich, Institute for Landscape Ecology and Resources Management, Justus-Liebig University, Giessen, Germany

Publication / Dissemination approved by technical committee members:

Christelle Pagotto, Veolia Water, Technical Direction, Saint-Maurice, France

Boris David, Veolia Water, Technical Direction, Saint-Maurice, France

Magali Dechesne, Veolia Environnement Recherche & Innovation (VERI), Paris, France

Emmanuel Soyeux, Veolia Environnement Recherche & Innovation (VERI), Paris, France

Nicolas Rampnoux, Veolia Environnement Recherche & Innovation (VERI), Paris, France

Guy Randon, Veolia Eau Région Ouest, Rennes, France

Lenore Tedesco, Center for Earth and Environmental Science, Department of Earth Sciences, Indiana University – Purdue University, Indianapolis, USA

Norbert Litz, Umweltbundesamt, Berlin, Germany

Bernard Sautjeau, Société d'Environnement, d'Exploitation et de Gestion de Travaux, St. Malo, France

Kai Schroeder, Kompetenzzentrum Wasser Berlin gGmbH, Berlin, Germany

Yann Moreau-Le Golvan, Kompetenzzentrum Wasser Berlin gGmbH, Berlin, Germany

Martin Bach, Institute for Landscape Ecology and Resources Management, Justus-Liebig University, Giessen, Germany

Caroline Guégain, Syndicat Mixte Environnement du Goëlo et de l'Argoat, Pordic, France

Deliverable number

Aquisafe 2 D 7.1

Abstract

The project Aquisafe assesses the potential of selected near-natural mitigation systems, such as constructed wetlands or infiltration,zones, to reduce diffuse pollution from agricultural sources and consequently protect surface water resources. A particular aim is the attenuation of nutrients and pesticides. Based on the review of available information and preliminary tests within Aquisafe 1 (2007-2009), the second project phase Aquisafe 2 (2009-2012) is structured along the following main components:

(i) Development and evaluation of GIS-based approaches for the identification of diffuse pollution hotspots, as well as model-based tools for the simulation of nutrient reduction from mitigation zones

(ii) Assessment of nutrient retention capacity of different types of mitigation zones in international case studies in the Ic watershed in France and the Upper White River watershed in the USA under natural conditions, such as variable flow.

(iii) Identification of efficient mitigation zone designs for the retention of relevant pesticides in laboratory and technical scale experiments at UBA in Berlin.

The present study focused on (i) and aimed at testing GIS approaches for the localization of critical source areas (CSAs) of diffuse NO_3^- pollution in rural catchments with low data availability as a basis for the planning of mitigation measures.

We tested a universal *GIS*-based approach, which is a combination of published methods. The five parameters *land use*, *soil*, *slope*, *riparian buffer strips* and *distance to surface waters* were identified as most relevant for diffuse agricultural NO_3^- pollution. Each parameter was classified into three risk classes, based on a literature review. The risk classes of the five parameters were then averaged in a GIS overlay in order to find areas with highest risk.

The Ic catchment in Brittany, France, served as a study site to test the applicability of the chosen approach. The result of the overlay was compared (a) with measured NO_3^- loads in seven subcatchments of the Ic catchment and (b) with the results of a previous analysis by the numerical model *Soil and Water Assessment Tool* (*SWAT*). Regarding (a) it was found that higher mean risk classes in a subcatchment correspond with higher measured NO_3^- loads. However, due to the small number of data points a reliable statistical analysis was not possible. Regarding (b), the plotting of the loads predicted by

SWAT against the mean risk class for the 32 SWAT subcatchments show a similar, but poorer relationship.

The GIS approach was further analyzed regarding its sensitivity to each of the parameters. The analysis showed that the method is not very sensitive to most of the parameters, i.e. risk class distribution (or the choice of CSA) does not change greatly if one parameter is omitted. Nevertheless, if data quality for some parameters is known to be low, sensitivity of the result to the parameter should be considered in addition.

In summary, it can be stated that the applied GIS overlay is a promising, easy to handle approach. First experiences on the Ic catchment indicate that GIS-based approaches can be robust, even for lower data availability. As a result, further work is suggested towards developing a universally applicable GIS method for nitrate CSA identification. Main points to be assessed are the number of classes, the necessary weighting of parameters and the best inclusion of different nitrogen pathways between field and surface water.

Acknowledgements

This work is based on data on the Ic catchment supplied by the Syndicat Mixte Environnement du Goëlo et de l'Argoat (SMEGA). Particular support was given by Caroline Guégain and Céline Quélo from SMEGA. For validation of results model results were supplied by Stefan Julich from the Institute for Landscape Ecology and Resources Management at the Justus-Liebig University. Language was significantly improved thanks to the review by Eva Niepagenkemper and Rae Winkelstein.

The work was carried out in the framework of a Masters thesis. Supervisors Prof. Dr. Köhler and Prof. Dr. Scholten at the University Tübingen are thankfully acknowledged for their support.

The report was written in the framework of the KWB project AQUISAFE, financed by Veolia Water.

Table of Contents

List of Figures

List of Tables

Abbreviations and Symbols

Abbreviations

AWC	Available Soil Water Capacity
C2	Subcatchment ‘Camet’
CLC	Coordinated Information on the European Environment Land Cover
CORINE	Coordinated Information on the European Environment
CSA	Critical Source Area
DEM	Digital Elevation Model
e.g.	for example
ER	Exchange Rate
ESRI	Environmental Systems Research Institute
EU	European Union
FIS-DQ	Fachinformationssystem Diffuse Quellen (Information System for Diffuse Sources)
G.E.	Subcatchment ‘Gué Esnart’
GIS	Geographical Information System
I2	Subcatchment ‘Ic Amont’
I4	Subcatchment ‘Ic Centre’
I6	Subcatchment ‘Ic Littoral’
i.e.	that is
K	Soil factor (Universal Soil Loss Equation)
L1	Subcatchment ‘Lantic’
MUNLV	Ministerium für Umwelt und Naturschutz, Landwirtschaft und Verbraucherschutz des Landes Nordrhein-Westfalen (Ministry of the Environment and Conservation, Agriculture and Consumer Protection of the German State of North Rhine-Westphalia)
nFKWe	nutzbare Feldkapazität im effektiven Wurzelraum (Root Zone Available Soil Water Capacity)

n. d.	no date
n. p.	no place
PW	Percolating Water
PWP	Permanent Wilting Point
R2	Subcatchment ‘Rodo’
RC	Risk Class
RZ_{eff}	Effective Root Zone
RZAWC	Root Zone Available Soil Water Capacity
S	Slope steepness factor (modified Universal Soil Loss Equation)
SC	Subcatchments (of the SWAT application)
SMCG/GOËL’EAUX	Syndicat Mixte de la Côte du Goëlo (Joint Commission of the Coast of Goëlo)
SMEGA	Syndicat Mixte Environnement du Goëlo et de l'Argoat (Environmental Joint Commission of the Goëlo and the Argoat)
SWAT	Soil Water and Assessment Tool
U	Land use factor (from modified Universal Soil Loss Equation)
US	United States
USA	United States of America
USDA	United States Department of Agriculture
USLE	Universal Soil Loss Equation
VS	Subcatchment ‘Ville Serho’
vTI	Johann Heinrich von Thünen-Institut
W	Watercourse factor (from modified Universal Soil Loss Equation)
WFD	Water Framework Directive
WHO	World Health Organization
Wpfl	pflanzenverfügbares Bodenwasser (Plant available soil water)

Scientific symbols and abbreviations

℃	Celsius
cm	centimeter
ha	hectar
km	kilometer
L	liter
m	meter
mm	millimeter
N	nitrogen
NH_4^+	ammonium
NO_2^-	nitrite
NO_3^-	nitrate
R^2	determination coefficient
yr	year
µm	micrometer
θ	slope angle

Chapter 1
Introduction

Typical measures for reduction of diffuse NO_3^- pollution aim (i) at avoiding NO_3^- leaching at its source, e.g., via an optimized fertilization by farmers or (ii) at reducing NO_3^- concentrations 'end-of-pipe' via water treatment at the waterworks. A third option (iii) that can supplement (i) is the placement of mitigation zones, such as constructed wetlands, before agricultural runoff reaches surface waters. Method (iii) is of particular interest in rural agricultural watersheds, where measures at the source are not sufficient to achieve the necessary raw water quality for drinking water production and a 'good status' according to the WFD. Option (iii) is investigated in the *Aquisafe 2* project. In order to maximize the effect of planned mitigation zones there is great interest in placing them in or downstream of critical source areas (CSAs or hotspots) of NO_3^- pollution. The present thesis is written within the scope of *Aquisafe 2*.

The aim of this work is the testing of *Geographic Information System (GIS)*-based approaches for CSA localization in rural catchments with low data availability as well as to analyze their utility. The idea of the tested GIS approaches is to provide a ranking of areas regarding their potential as NO_3^- sources, but not to predict NO_3^- concentrations or loads in surface waters. The tested approaches focus on small to medium size catchments with fairly homogeneous climate conditions. The rural Ic catchment in Brittany, France, serves as a case study. Detailed catchment characteristics are described in Chapter 2.

In a previous project, *Aquisafe 1*, different numerical methods for the determination of CSAs for NO_3^- pollution were assessed. The study included the comparison of several numerical physically-based models (Strube 2009) and the application of the numerical, basin-scale hydrological model *Soil and Water Assessment Tool (SWAT)* to the Ic catchment in France (Julich *et al.* 2009). Commonly, such numerical models are used for a scientific or applied assessment of the involved processes or for a detailed scenario analysis (Skop and Sørensen 1998). However, in many catchments the application of numerical models is limited, because of their high data requirements. Moreover, the application of SWAT or similar models is very time-consuming and requires experienced users. Therefore, alternative methods with less data and time requirements can be very useful screening tools to find CSAs in catchments. Such methods were reviewed to reveal which methods provide a promising alternative to numerical models for a first assessment of CSAs (Bugey 2009). Many of these approaches use GIS (e.g., Bae and

Ha 2005; Jordan 1994; Munafo et al. 2005); however, all of them are site-specific and therefore not transferable to other catchments. An advantage of these non-numerical GIS-based approaches is that they often reduce costs, because further investigations and measures against diffuse pollution can be focused directly on the CSAs.

Based on methods described in Bugey (2009), a GIS-based approaches for CSA analysis are tested and combined in this work and exemplified for the Ic catchment.

Following an introduction of the study site (Chapter 2) the tested approaches are explained in detail and exemplarily applied to the Ic catchment (Chapter 3). The results for the Ic are validated in Chapter 4. Finally, conclusions and recommendations for the future development of a universal GIS method for CSA identification are given (Chapter 5).

Chapter 2
The study site

2.1 Description of the study site

The Ic catchment is located in the north of the department Côtes-d'Armor in Brittany, France. It covers an area of 92 km² and the elevation ranges between 4 meters above sea level in the north-east and 206 meters above sea level in the south (Julich *et al.* 2009).

The climate is temperate oceanic with a strong influence of the Atlantic Ocean leading to relatively warm winters and relatively cool summers. The mean temperature is 10.5°C and the annual precipitation varies between 750 and 1000 mm. The hydrological water balance shows that groundwater recharge does not takes place between May and August.

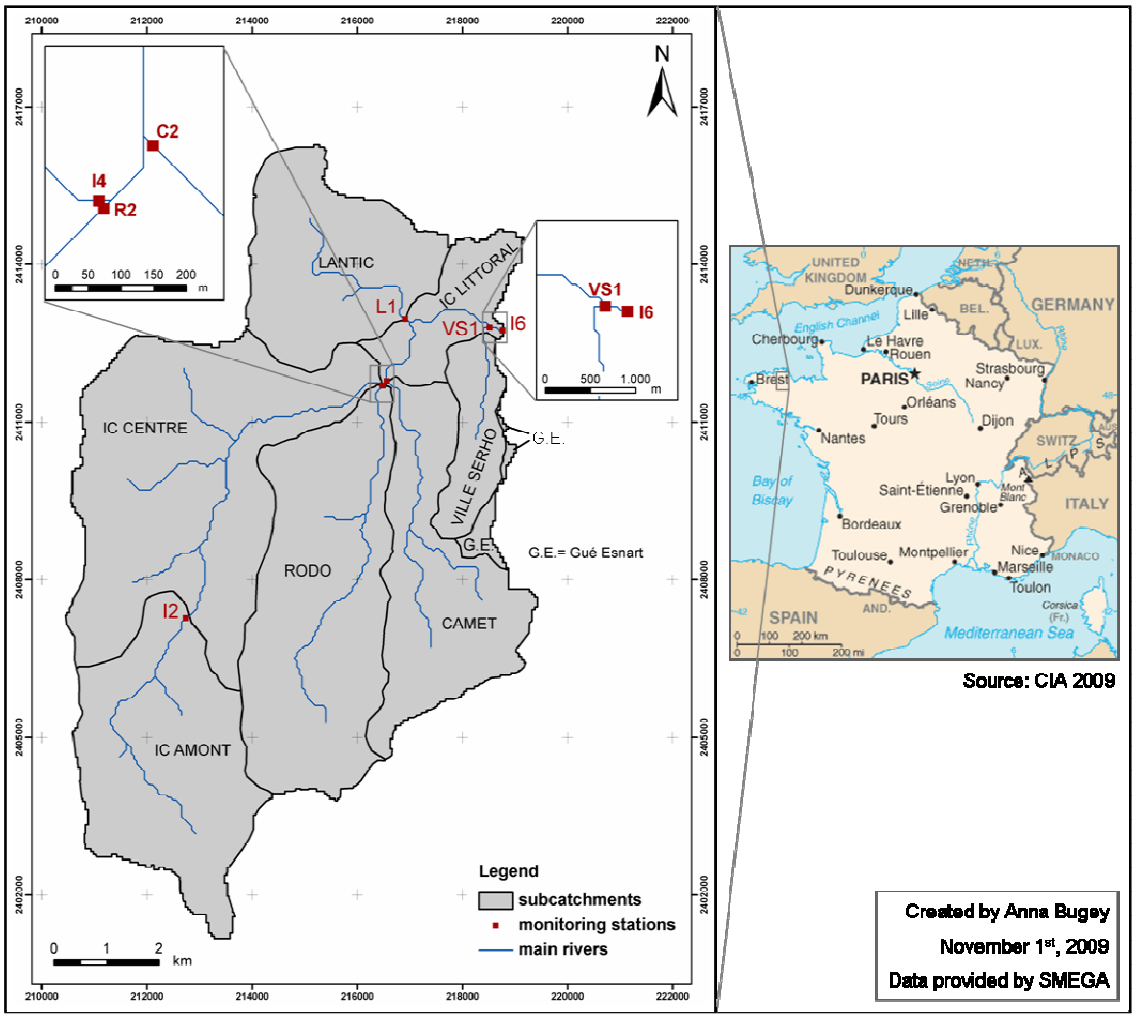

Figure 1. The Ic catchment in France with subcatchments and monitoring stations.

The catchment is subdivided into the seven subcatchments Camet, Ic Amont, Ic Centre, Ic Littoral, Lantic, Rodo, Ville Serho (Figure 1, for practical reasons the subcatchments are abbreviated with the names of the according stations in the figures of Chapters 3.4 and 4). Investigations of the pathways of NO_3^- fluxes via hydrograph analysis in *Aquisafe 1* came to the conclusion that the subcatchments Camet, Ic Amont, Ic Centre, Ic Littoral and Rodo are influenced by groundwater, while Lantic and Ville Serho are dominated by surface runoff. Ic Centre and Ic Littoral are influenced by upstream subcatchments, so the dynamics here could not be analyzed reliably from the hydrograph.

The rivers depicted in Figure 1 have a length of about 48 km. For clarity reasons, Figure 1 shows only the main river network in the catchment and does not include smaller streams and artificial ditches, which were, however, included in the analyses of this work. The average flow at the outlet of the catchment (station I6; Figure 1) is 0.66 m^3s^{-1}.

The catchment is located within the Armorican Massif. The most upstream part of the Ic catchment is dominated by acid magmatic rocks followed by basic magmatic rocks further downstream. The intermediate section of the catchment is composed of metamorphic rock, such as mica schist and amphibolites. The bedrock in the most downstream part of the catchment in the north-west comprises schist formations of the Upper Brioverian. The floodplains of the river are dominated by alluvium (SMCG/GOËL'EAUX 2007).

The predominant soil texture in the Ic catchment is silt loam in the floodplains and sandy silt in the remaining areas (see Figure 2; for more detailed information on the soil texture types see Chapter 3.3.2). The soil depth in the northern parts of the catchment is predominantly less than 60 cm, while in the south most soils are deeper than 60 cm.

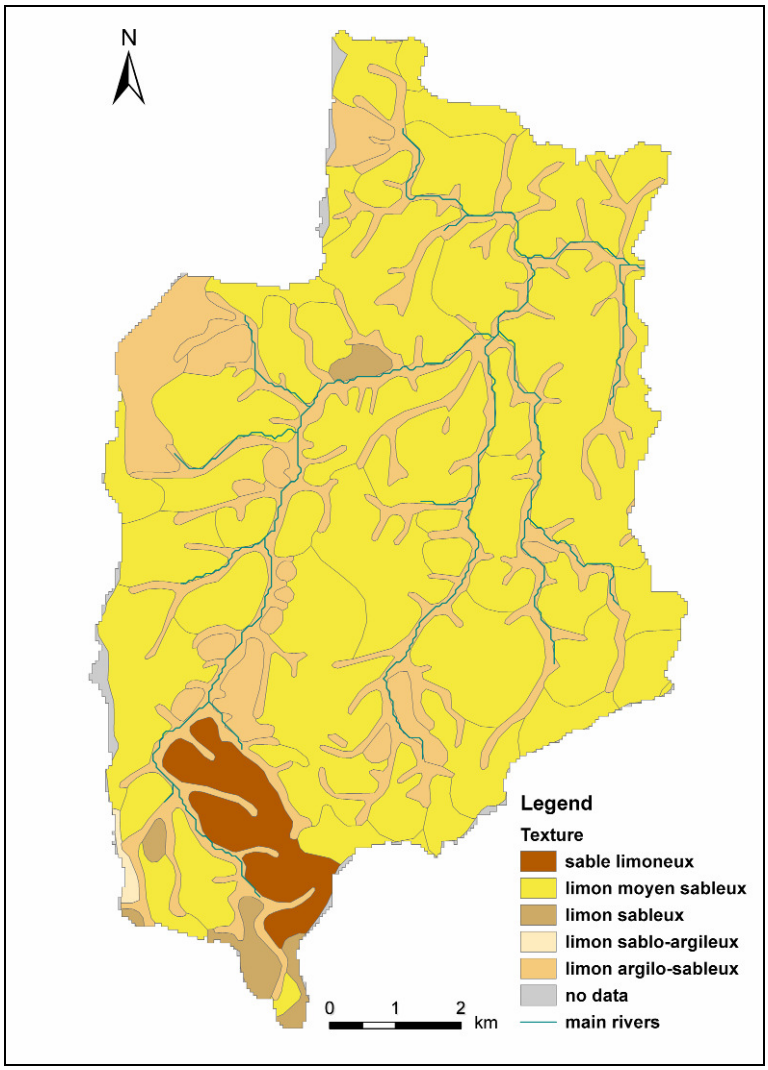

Figure 2. Soil texture map (Source : BDPA-SCET AGRI, 1987). Note that French nomenclature is used because of different classification in English-speaking countries.

Land use in the Ic catchment is clearly dominated by agriculture (Figure 3). Cropland makes up about 64 % of the catchment, while grassland and forests account for about 20 % and 16 %, respectively. Major crops in the catchment are cereals, rapeseed, corn and vegetables (Figure 3). Due to the intensive crop production and animal husbandry NO_3^- concentration in the river exceeds 50 mg NO_3^- L^{-1} almost year-round (Figure 4). Since the area has no major aquifers, river water was used for drinking water production until the beginning of 2009. Because of high NO_3^- levels the waterworks were closed down in order to avoid EU fines (INRA 2008).

Figure 5 (see p. 13) shows that apart from the main rivers (Figure 1), the stream network in the catchment comprises a great number of smaller water bodies. Many of these are artificial ditches used for drainage of agricultural cropland.

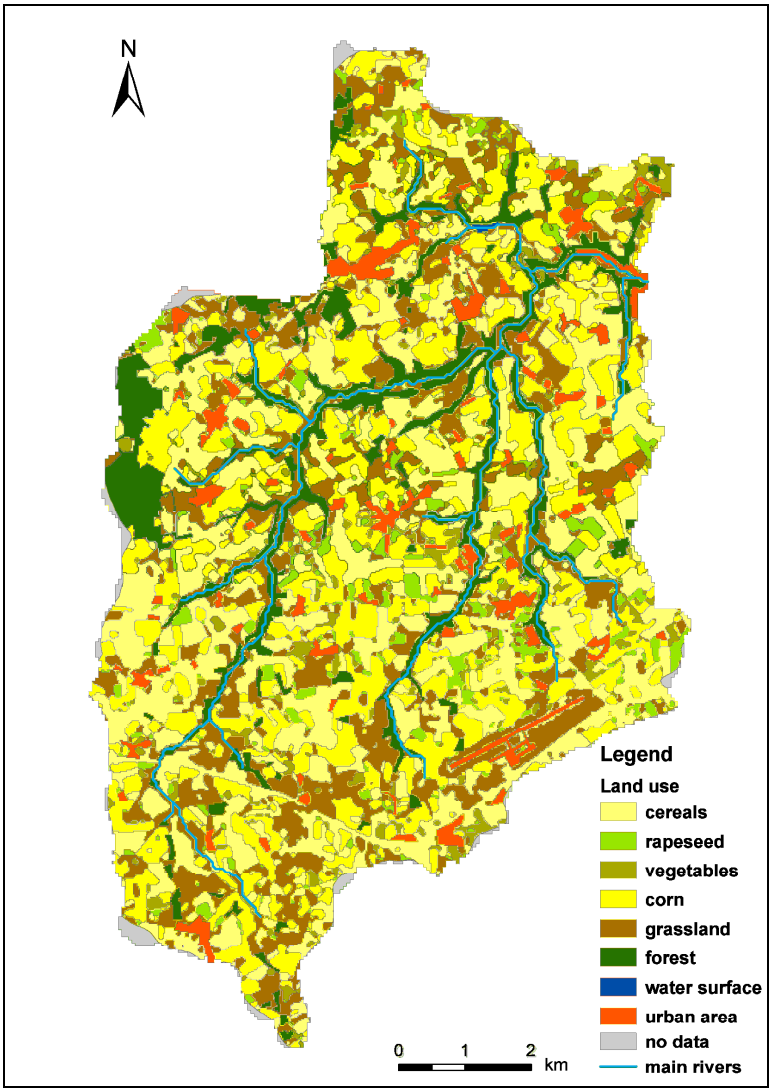

Figure 3. Land use in the Ic catchment in 1996/1997 (Source: Arerial Photographs processed by the Conseil général des Côtes d'Armor).

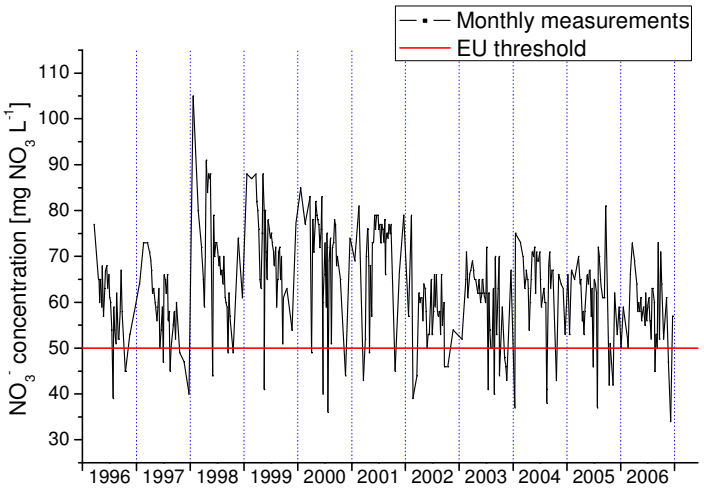

Figure 4. Monthly measurements of NO_3^- concentrations at station I6 (Figure 1), close to the mouth of the Ic. The red line depicts the EU threshold of 50 mg NO_3 L^{-1}.

2.2 Available Data

Spatial data were provided digitally by the Syndicat Mixte Environnement du Goëlo et de l'Argoat (SMEGA). These include:

- a 50 meter digital elevation model (DEM 50; source: IGN 2003 „Bd Alti 2003"),
- a land use map (Figure 3),
- a soil texture map (Figure 2),
- a soil depth map,
- a stream network map digitized from aerial photographs (Figure 5).

The land use map was digitized from aerial photographs taken in 1996/97 by the Conseil général des Côtes d'Armor. The soil texture and soil depth map is based on the soil map by BDPA SCET AGRI (1987).

Discharge rates and NO_3^- concentrations were measured monthly at the seven monitoring stations from 1996 until 2007 and provided by SMEGA. The stations are depicted in Figure 1.

The outer catchment boundaries used in this study were delineated from the DEM 50 by Julich *et al.* (2009). These boundaries differ slightly from the ones in the original data by SMEGA. However, it was decided to use the ones by Julich *et al.* (2009), because they delineate the catchment drained by the most downstream monitoring station at which both NO_3^- concentrations and discharge have been measured (I6; Figure 1). The

subcatchments from SMEGA included an eighth catchment (Gué Esnart), which joins the sea directly and is excluded from this study. However, the DEM 50 based catchment overlaps in the east with some parts of the subcatchment Gué Esnart (Figure 1).

Data on the results of the SWAT analysis by Julich *et al.* 2009 were provided by Stefan Julich.

There is only one meteorological station in the catchment. Therefore, detailed climatic variations cannot be identified for the catchment. A maximal gradient in precipitation of ~80 mm yr^{-1} (data by SMEGA) was estimated between the coastal area and the backcountry of the Ic. Given the low gradient and low differences in elevation, climate does not have to be considered.

2.3 Pre-processing of data

GIS functions using a DEM as input data require the creation of a 'depressionless' DEM (Environmental Systems Research Institute 2005a). This was performed for the DEM 50 in this study and the resulting depressionless DEM was used for all GIS functions which utilize a DEM. A flow chart of the creation of the depressionless DEM can be found in the appendix (A 1.).

Loads were calculated from concentrations [mg L^{-1}] and discharge [m^3 s^{-1}] for each monitoring station and date (in the following referred to as "measured NO_3^- loads"). The mean load for each subcatchment was calculated from ten years of monthly loads (Figure 5). In order to obtain the effective loads of the subcatchments Ic Centre and Ic Littoral, the loads of the stations upstream of I4 and I6 had to be subtracted from the loads at those stations. It has to be noted that NO_3^- loads, based on monthly measurements can contain significant errors, because e.g., effects of storm water events are not fully accounted for.

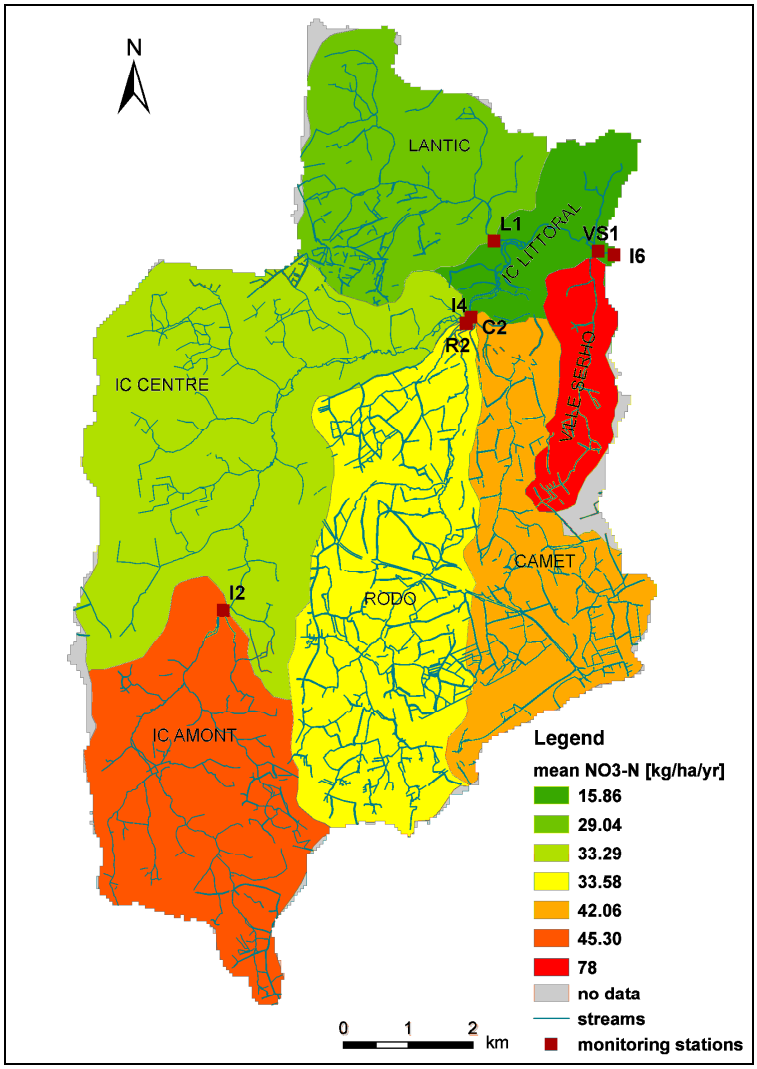

Figure 5. Mean measured NO_3^--N loads in per sub-catchment (data provided by SMEGA).

Chapter 3
Methodology and Application

3.1 General Approach

The main goal of this work is the testing of a GIS approach which provides a simple way to identify CSAs that contribute most to high NO_3^- concentrations in surface waters. This identification of CSAs is important in order to place mitigation measures effectively. Especially in rural catchments the data situation often does not allow complex and data intensive methods (e.g., Maillard and Pinheiro Santos 2008). The chosen approaches will be applied exemplarily to the Ic catchment in France (see Chapter 2). The results are compared with limited measurements of NO_3^- loads, as well as the more complex SWAT analysis performed on the Ic catchment by Julich *et al.* (2009).

A GIS-based overlay was chosen because it is easy to add and remove single layers depending on their availability in a given catchment. This is particularly important in rural catchments where the data situation can vary substantially between different catchments. Thereby transfer to other catchments is easily possible, which would be an important requirement of a potential method. Certainly, quality of results remains to be assessed. Moreover, GIS allows a good visualization of results. A further advantage is that knowledge on GIS is widespread and most engineering companies can apply GIS overlay individually. The ArcGIS software by ESRI (Environmental Systems Research Institute 2005b) was chosen because of its common use. Transfer to other GIS applications is possible if these include the relevant functions. In this study the following steps were performed:

1. Identification of parameters: Spatial parameters, which are important factors for NO_3^- export, are identified from literature (Chapter 3.2).
2. Classification: Each parameter is classified into three risk classes regarding NO_3^- export (1 = low risk, 2 = medium risk and 3 = high risk (Chapter 3.3)).
3. Application to single parameters: The risk classes are applied individually to single parameters in the Ic catchment in France (Chapter 3.3).
4. Overlay: The risk class maps for the single parameters are combined in ArcGIS and analyzed regarding the information gained by the overlay (Chapter 3.4).
5. Comparison: In order to understand the benefit of such an approach, the results of the overlay are compared with measured NO_3^- loads and with the results of the

SWAT analysis (Chapters 4.1.1 and 4.1.2). Moreover, sensitivity of the overlay to single parameters is assessed (Chapter 4.2).

In order to keep the approach as simple as possible, all parameters are classified into three risk classes. This facilitates the applicability to a great number of catchments. The definition of the risk classes for the different parameters is based on an intensive literature study in Chapter 3.3.

In the present work, risk classes are defined by relating the three risk classes to the full range of possible values for this parameter (independent from the range of values found in the given catchment). This approach makes the classes applicable to many catchments, but, if the range of values is small, it is possible that only one risk class occurs in a specific catchment. The problem could be circumvented by relating the three risk classes to the range of values present in a specific catchment. Here, the difficulty is (a) that the classification is not comparable to other catchments (e.g., catchments with generally high or low NO_3^- pollution would cover the same range of risk classes) and (b) that the impact of uniform parameters may be overestimated (e.g., if a catchment has a low risk of NO_3^- export according to its slope, the slope layer will still be divided into three risk classes, which leads to an overestimation of the risk in this layer). Given the restrictions (a) and (b), risk classes were defined universally in this test.

Furthermore the respective class width needs to be chosen. The basis for the choice of risk classes differs among the parameters and is described in detail in Chapter 3.3.

3.2 Parameter selection

The selection of the single parameters is based on a literature study on factors influencing diffuse NO_3^- pollution of surface waters. Factors, commonly considered by GIS approaches regarding NO_3^- export from a given surface can be distinguished into three groups (Bugey 2009):

(1) Factors controlling sources of NO_3^- (such as fertilizer application or atmospheric deposition)

(2) Factors controlling transport of NO_3^- from fields to surface water (such as soil texture)

(3) Factors controlling NO_3^- retention between field and surface water (such as presence of riparian buffer strips)

In order to maximize transferability of the factors, existing approaches of catchment analysis and CSA identification (MUNLV 2005; Kuderna *et al.* 2000; Trepel and Palmeri

2002) were broken down to the most basic and readily available parameters. It was attempted to separate influencing parameters as well as possible, i.e., preferably the chosen parameters should not have the same input data. The following five parameters were chosen and discussed in detail in Chapter 3.3:

Group (1): - *Land use*

Group (2): - *Soil*

- *Slope steepness*

Group (3): - *Riparian buffer strips*

- *Distance to surface waters*

In addition to the above parameters climate factors are considered by some CSA identification methods (e.g., Jordan 1994; Schlecker 2003). They are excluded from this study, because they are regarded as homogeneous within most small to medium size catchments. However, in large or alpine catchments with variable climate conditions, parameters, such as precipitation and evaporation may have to be taken into account. Thus, the described approach cannot be applied directly to those catchments; in most cases catchments could be split up into subcatchments with homogenous climatic conditions.

In the following section each parameter is discussed along the following structure:

1. Importance of the parameter
2. Definition of risk classes
3. Data requirements
4. Application to the Ic
5. Discussion of the parameter

3.3 Application to single parameters

3.3.1 Land use

Importance of parameter land use

A number of studies have shown that land use is one of the governing parameters influencing NO_3^- export from land surfaces (e.g., Beaulac and Reckhow 1982; Crétaz

and Barten 2007; Maillard and Pinheiro Santos 2008; Dise and Wright 1995). The main reasons for differences in NO_3^- export between land use types are different amounts of N-surplus, i.e., the difference between N-input on the one side (i.e., fertilizer and atmospheric deposition) and the N-storage (i.e., via soil storage or plant uptake) as well as N-export via harvest on the other side. The N-surplus is lost to groundwater and surface water.

Under naturally vegetated land cover, NO_3^- enriched water is released slowly to the rivers due to plant uptake and soil storage (e.g., McCulloch and Robinson 1993). Land use changes resulting from agricultural usage can lead to elevated NO_3^- input on (cultivated) land surfaces, higher share of surface runoff and more erosion, which in turn causes an increase in NO_3^- input into surface waters (e.g., McCulloch and Robinson 1993; Kaste *et al.* 1997; Magdoff *et al.* 1997; Beaulac and Reckhow 1982).

Definition of risk classes

Studies on the relation between land use and NO_3^- export have shown that *cropland* is the land use that contributes most to NO_3^- eluviations into surface waters (e.g., Basnyat *et al.* 2000; Magdoff *et al.* 1997). The predominant NO_3^- input on agricultural cropland is organic and inorganic fertilizer application (Maillard and Pinheiro Santos 2008; Mattikalli and Richards 1996; Basnyat *et al.* 2000; Foster *et al.* 1989). Among agricultural areas there are differences in NO_3^- export depending on farming methods and type of crop (Magdoff *et al.* 1997; Di and Cameron 2002).

Grassland can generally store more NO_3^- than agricultural fields due to its higher humus contents (Franko *et al.* 2001, p.169). Some grassland is fertilized directly by farmers, some is fertilized indirectly by grazing cattle and some is not fertilized at all. Therefore NO_3^- export from grassland varies greatly depending on fertilizer input and type of use, e.g., grazing or mowing (Franko *et al.* 2001, p.169). Given the higher N storage capacity of grasslands, turning of grassland into cropland can lead to a high, sudden N loss for several years (Nieder 2009; Di and Cameron 2002).

Forests receive most of their N input from atmospheric deposition (Wendland *et al.* 1993), which is the governing factor for N leaching in this land use type (Dise and Wright 1995; Franko *et al.* 2001, p. 169; Schulze *et al.* 1989). The same is true for other uncultivated areas. Up to a certain amount of N input, natural ecosystems have the capability to immobilize N by microbial processes and incorporate N into biomass (e.g., Franko *et al.* 2001, p. 169). Critical loads indicate how much of a substance can be deposited without causing adverse long-term effects to the ecosystem itself and to neighboring ecosystems, namely surface waters and groundwater (Umweltbundesamt

2008a). According to the German Environmental Protection Agency (Umweltbundesamt 2008b) depending on the site an atmospheric deposition of 5 to 20 kg N ha^{-1} yr^{-1} is considered as uncritical for the N-cycle of forest ecosystems. In Germany, atmospheric N deposition is usually estimated at 20-30 kg N ha^{-1} yr^{-1}; however some studies from Germany and other European countries suggest that atmospheric deposition can amount up to 60 kg N ha^{-1} yr^{-1} (e.g., Weigel *et al.* 2000; Franko *et al.* 2001, p.169). Long-term exceeding of critical loads leads to export of NO_3^- via percolating water. Especially in forests, the soil gets N-saturated over the time, so after humus build-up, annual N storage decreases drastically (Umweltbundesamt 2008c; Umweltbundesamt 2008b; Aber *et al.* 1989). Under saturated conditions, 50 % of the (atmospheric) N input is washed out from forest soils (Wendland *et al.* 1993). In this case it is possible that N export from forests can be even higher than from agriculturally used grassland as Franko *et al.* (2001) found. However, information on N-saturation of soils is not widely available. As a result, it is not considered in the class definition below.

Small areas with impervious surfaces, such as roads, can be considered to have a low susceptibility for NO_3^- export in a predominantly rural watershed. Since this study is directed towards rural watersheds it does not consider the case of larger urban areas. However, it should be mentioned that large urban areas can be an important N source even in the absence of point source effluents, mostly via input from vegetation (pollen or tree leaves) from parks and alleys (Heinzmann 1993).

Resulting from the performed literature study, the parameter *land use* was classified into the three categories ‘cropland’ (risk class 3), ‘other fertilized areas’ (risk class 2), such as fertilized grassland and grazed pastures, and ‘unfertilized areas’ (risk class 1), such as forests or uncultivated grassland (Table 1). A similar distinction was used by Auth *et al.* (2005) who found N losses mostly between 10 and 40 kg N ha^{-1} yr^{-1} for agricultural cropland, whereas 5 kg N ha^{-1} yr^{-1} were estimated for non-cultivated areas, such as forests. Similarly, Baß *et al.* (2005) found average concentrations of 10 mg NO_3^- L^{-1} in groundwater with a catchment dominated by forest and grassland, but 21 to 25 mg NO_3^- L^{-1} under cropland. The classification in the present study further agrees with a review by Di and Cameron (2002), who assessed forest as least contributive (N-loss 5 to 15 kg N ha^1yr^{-1}), followed by cut grassland (6 to 49 kg N ha^{-1} yr^{-1} for intensive fertilization), cropland (8 to 107 kg N ha^{-1} yr^{-1}) and horticulture (up to 300 kg N ha^{-1} yr^{-1}).

As stated above, significantly lower N loss was found for cut grassland than cropland, even if same amounts of fertilizer/manure were applied. However, if fertilized grasslands were grazed in addition, N loss was similar as for cropland (Di and Cameron 2002). In practice, grassland is usually either fertilized and cut or grazed on. Moreover, in most

cases, more fertilizer is applied to cropland than grassland. As a result, cultivated grassland is classified as class 2, even if some specific areas may correspond to class 1 or class 3. If possible, non-agricultural grassland should be distinguished in class 1.

Land cover information can be obtained from the CORINE Land Cover (CLC) project which is part of the Coordinated Information on the European Environment (CORINE) program of the EU and provides land cover information for all EU member states in the resolution of 1:100 000. The data can be downloaded from the website of the European Environment Agency (European Environment Agency 2000).

Table 1. Risk classes for the parameter *land use*.

Risk class	Land use
1	unfertilized areas (forests, non-agricultural grasslands, small impervious areas)
2	other fertilized areas (grazed or fertilized grasslands, fertilized forests)
3	cropland

Data requirements (land use)

(a) Requirements: spatial distribution of land use (e.g., from CORINE land cover at a resolution of 1:100,000). Distinction among 'cropland', 'grassland' and 'unfertilized areas' according to Table 1.

(b) Additional data: In some catchments, large areas of unfertilized grasslands or natural wetlands may exist. If spatial information is available these areas should be included in risk class 1.

Application to the Ic catchment

Data on agricultural fields was available for 1996/97 in the categories vegetables, cereals, rape and corn (Table 2; Figure 3). For this test application this high resolution map was used. In real application an eight year old land use map is critical and CORINE land cover (with lower resolution) might be preferred. According to Julich *et al.* (2009) corn and wheat receive on average 203 kg N ha^{-1} yr^{-1} and 173 kg N ha^{-1} yr^{-1}, respectively.

In the Ic catchment the fertilizer input on grassland varies to a great extent. 80 % of the grassland areas are estimated to receive a similar amount of fertilizer as the agricultural fields while the remaining 20 % do not receive any fertilizers (C. Quélo, personal communication). From the available spatial data, differentiation between fertilized and unfertilized pasture is not possible. Therefore no distinction was made in the risk classification and both were placed in the medium risk class.

Table 2. Original land use categories for the Ic catchment and their assigned risk classes.

Original land use category	% of total area	Risk class
Cereals	31,8	3
Corn	24,5	3
Rape	4,1	3
Vegetables	4,7	3
Grassland	16,3	2
Forests	12,0	1
Urban/impervious areas	6,6	1
Water surfaces	0,04	1
Total	100	-

Figure 6 shows the resulting risk map for the parameter land use applied to the Ic. The predominance of agricultural cropland (red), which covers about 64 % of the total catchment (Table 3), underlines the pressure on the Ic from agricultural sources. Although there are differences among the relative importance of the three classes, each class is distributed fairly evenly over the entire catchment. As a result, distinct CSAs cannot be determined conclusively from the analysis of this single parameter. Risk class 1 (about 16% of the catchment) is mainly present along the streams, in areas too humid or too steep to be cultivated.

The flow chart of the steps performed for the parameter *land use* in the Ic catchment can be found in the appendix (B 1.).

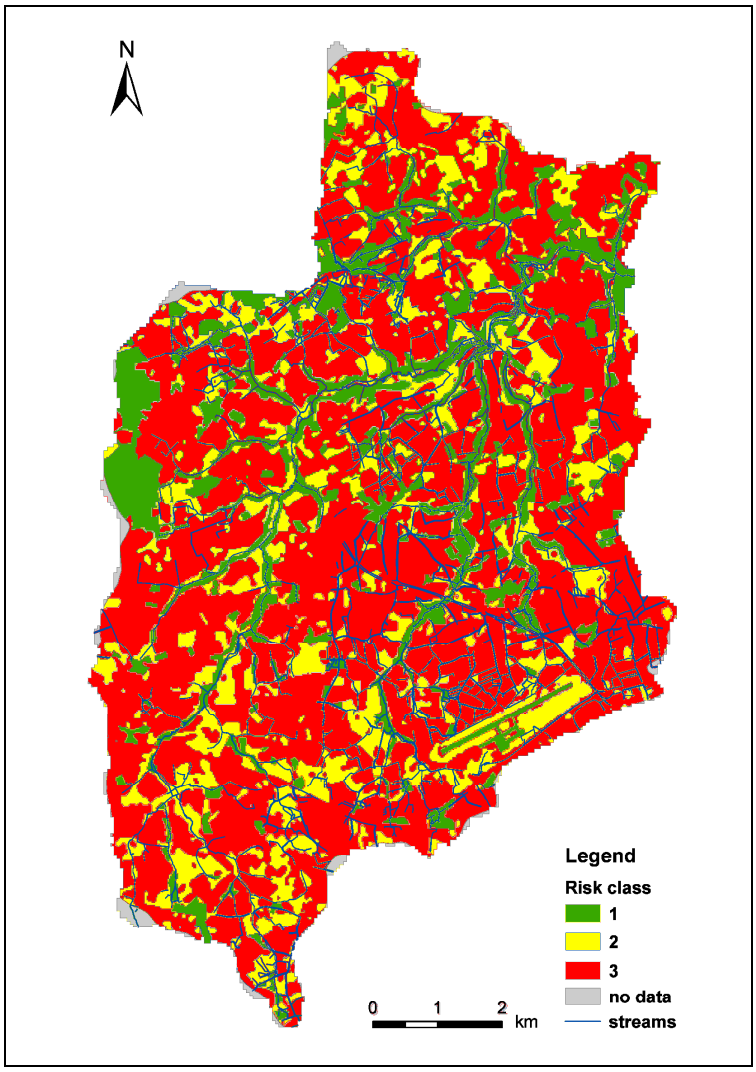

Figure 6. Risk map of the parameter *land use*.

Table 3. Percentages of risk classes for the parameter *land use*.

Risk class	Percentage of total area [%]
1	16.3
2	20.1
3	63.5

Discussion of the parameter land use

Most studies show significant differences in N-loss among different crops and agricultural practices. Nevertheless no distinction is made in the classification since (i) actual N loss is case specific, (ii) often spatial details on crop types are not available and (iii) average N loss from agricultural fields is clearly higher than from other land uses.

The quality of the result depends to a great extent on the resolution of the data and date of recording. Obviously, land use is subject to changes and consequently quality of allocation of land use risk classes increases with newer data. Nevertheless, the rough risk classes defined above are believed to be more robust than detailed information on cultivated crops.

The categories chosen for the three risk classes are based on the results of various studies on the effect of land use on NO_3^- loss and can be regarded as reliable. However, concerning the application to the Ic catchment, the placement of all grassland in the medium risk class might lead to an overestimation of N loss for the 20 % of unfertilized grassland.

3.3.2 Soil

Importance of parameter soil

Soil properties are a major control on the pathways of water on its way to the rivers and streams. Generally, sandy soil and gravel lead to subsurface flow, while clay facilitates surface runoff (Scheffer 1989, p. 171). In a detailed study of the German part of the large Elbe River (German catchment ~100000 km^2) groundwater pathway was the dominant transport pathway of nitrogen, accounting for 66 % of diffuse agricultural nitrogen emissions, followed by 26 % from tile drainage and 5 % from surface runoff Arbeitsgemeinschaft für die Reinhaltung der Elbe (2001). The results underline the importance to include groundwater pathway for nitrogen, even if risk for surface water pollution is focused on. In this study, soil is considered with regard to NO_3^- leaching into subsurface and groundwater, which is typically connected to surface waters at some point. This means that overland flow is neglected in the parameter *soil*, but considered in the parameter *slope*.

The risk of NO_3^- leaching into groundwater is assessed by using the parameter *Root Zone Available Soil Water Capacity (RZAWC)*, i.e. the water volume available to plants in the root zone. This parameter is mainly governed by soil texture and reflects the

exchange rate of water in the soil, which NO_3^- leakage is closely linked to. It can be obtained from the soil texture data which is generally one of the parameters available even in catchments with little soil data. Hereafter, the parameter *soil* and *RZAWC* are used synonymously.

Definition of risk classes

The higher *RZAWC*, the more water can be retained in the soil, leading to a lower volume of water percolating to the groundwater and finally to a lower risk of NO_3^- leakage. The overall risk of NO_3^- leakage is therefore inversely proportional to *RZAWC* and typically defined through the exchange rate (*ER*):

$$ER = \frac{PW}{RZAWC} \text{ [\% yr}^{-1}\text{] (Kuderna } et\ al. \text{ 2000),} \qquad (1)$$

where *PW* [mm yr^{-1}] = amount of percolating water (= gravitational water) and *RZAWC* [mm] = root zone available water capacity (German: *nutzbare Feldkapazität im effektiven Wurzelraum*).

Although *PW* is a complex parameter, it is typically estimated empirically from climate factors such as precipitation and humidity (e.g., Renger 2002; Kuderna *et al.* 2000). As previously discussed, this work focuses on small to medium-sized catchments for which climate (and thus *PW*) is assumed to be constant. Therefore only *RZAWC* is considered for this study. It is mainly dependent on soil texture (Scheffer 1989, p.199) and used to represent the amount of water available for plants (German: *pflanzenverfügbares Bodenwasser*; W_{pfl}) in terrestric soils not affected by groundwater. In hydric soils, the capillary rise needs to be considered. In this case capillary rise [mm] has to be added to *RZAWC* (Ad-hoc-Arbeitsgruppe Boden 2005, p.356). For many catchments relevant to this study, information on groundwater influence on the soils is not available. As a result, the capillary rise is neglected in the following.

RZAWC is defined as the available soil water capacity (*AWC* [mm cm^{-1}]; German: *nutzbare Feldkapazität*) times the effective root zone (RZ_{eff} [cm]; German: *effektiver Wurzelraum*):

$$RZAWC = AWC * RZ_{eff} \qquad \text{[mm] (Ad-hoc-Arbeitsgruppe Boden 2005, p.356)} \qquad (2)$$

Both *AWC* and RZ_{eff} can be determined using data on soil texture and effective density. The former should be available as a standard soil parameter in most catchments, while the latter can be assumed medium if no further information is available.

AWC is the water available for plants in mm per cm soil and defined as

$AWC = FC - PWP$ [mm cm^{-1}] (Scheffer 1989, p.197), (3)

where *FC* [mm cm^{-1}] = field capacity and *PWP* [mm cm^{-1}] = permanent wilting point. *AWC* depends on the soil texture and the crop (Ley *et al.* 1994). However, detailed information on crops will not be available in many catchments.

RZ_{eff} is the calculated depth of the soil zone, in which the *AWC* can be exploited by annual agricultural crops (Ad-hoc-Arbeitsgruppe Boden 2005, p.355). It influences how much water can be extracted from the soil by plant roots and depends on soil type and vegetation for deep soils (Ad-hoc-Arbeitsgruppe Boden 2005, p.355). Vegetation was not considered in this study, because it is partly included in the parameter *land use*. In some areas the actual soil depth is lower than the RZ_{eff} obtained from literature, i.e., the soil depth is the limiting factor for roots rather than soil type. In such cases the actual soil depth should be considered instead of RZ_{eff}. The shallower the soil, the less water can be stored (Ley *et al.* 1994). If soil depth is unknown for a catchment RZ_{eff} literature data may be used directly. Table 4 shows *RZAWC* and RZ_{eff} in relation to soil texture for the German classification system. It has to be noted that this relation to soil texture depends on the soil texture classification system used in the country in question. Attention should also be paid to the differing boundaries between soil texture classes (clay, silt, sand) in different countries. For instance, grains are considered to be ‘sand’ for grain sizes > 50 µm in France and the US but for sizes > 63 µm in Germany. Therefore values for *AWC* and RZ_{eff} should be obtained from sources referring to the same system. The translation from one system to another is prone to error. Besides the noted general classifications on country level, locally adapted *AWC* and RZ_{eff} versus soil texture relationships are sometimes available from soil maps. In this case the local information should be used.

Despite local differences, Table 4 is reasonably representative regarding tendencies of broad soil texture classes. For instance, silt is generally the soil texture with the highest *RZAWC* values, while clay and sand have lower values. For clay, this is due to a higher number of micro-pores (<0.2 µm) which retain water more strongly, so that less water is available for plants. Big pores in sand soils lead to high water losses due to gravitation. For the following approach, risk classes for *RZAWC* were chosen according to the German Soil-Scientific Mapping Directive (Ad-hoc-Arbeitsgruppe Boden 2005; see Table 5). The six original categories in Table 5 were reclassified into three classes in Table 6.

Table 4. Average *RZ_{eff}* and *RZAWC* related to soil texture (translated from Scheffer 1989, p. 199, Table 63).

Soil texture	Average RZ_{eff} [dm]	RZAWC [mm]
Coarse sand	5	30
Medium sand	6	55
Fine sand	7	80
Loamy sand	7	115
Silty sand	8	140
Loamy silt	11	220
Sandy loam	9	155
Silty loam	10	190
Clay loam	10	165
Loamy and silty clay	10	140

Table 5. Classification of *RZAWC* values in the Soil-Scientific Mapping Directive (adapted from Ad-hoc-Arbeitsgruppe Boden 2005, Table 80).

Classification	Level	RZAWC
Very low	1	< 50
Low	2	50 - <90
Medium	3	90 - <140
High	4	140 - < 200
Very high	5	200 - < 270
Extremly high	6	≥ 270

Table 6. Risk classes for the parameter *RZAWC*.

Risk class	RZAWC value	Original class from Table 5
1	≥ 140	High, very high, extremely high
2	90 - <140	Medium
3	< 90	Low, very low

Data requirements

(a) Requirements: soil texture; table to look up *AWC* and RZ_{eff}

(b) Additional data: soil depth

Application to the Ic

For the Ic case study the soil texture map from BDPA SCET AGRI (1987) and the soil depth map provided by SMEGA are used. *AWC* is obtained from local information in the supplement of the official soil map of the Departement des Cotes du Nord (BDPA SCET AGRI 1988). Minimum and maximum RZ_{eff} are based on a table from the Chambre d'Agriculture de l'Aisne (2007) which refers to the French soil classification system.

The provided soil depth data distinguishes only between soils shallower than 60 cm and deeper than 60 cm. For the shallow soils the actual soil depth is taken into account when determining the parameter *RZAWC*, since 60 cm is less than the RZ_{eff} for all soil types in the Ic catchment. For this study the five soil texture types present in the catchment are each subdivided into the categories ‘less than 60 cm’ and ‘deeper than 60 cm’ resulting in ten different soil classes in total (see Table 7).

In order to obtain *RZAWC*, minimum and maximum RZ_{eff} (Chambre d'Agriculture de l'Aisne 2007) and actual soil depth, respectively are multiplied with *AWC* from BDPA SCET AGRI (1988).

For the shallow soils < 60 cm actual soil depth is considered to be between 0 and 60 cm (minimum and maximum value, respectively). Results are summarized in Table 7, a more detailed overview on the calculations performed can be found in the appendix (B 2.). In some cases the resulting *RZAWC* ranges overlap with two of the risk classes defined in 4.1.1 (Table 6). These soil types are assigned the risk class with the predominant overlap and are marked with an asterisk in Table 7. Table 7 shows all ten soil classes found in the Ic catchment including the risk classes they are assigned. The steps performed in the GIS can be found as a flow chart in the appendix (B 3.).

Table 7. Soil classes in the Ic catchment, their textures and according risk classes.

Soil class	Soil texture (French)	Soil texture type (Engl.)[1)]	Soil depth [cm][2)]	*RZAWC* [mm][3)]	Risk class
SL	Sable limoneux	Loamy sand	> 60	80 – 90	3
SL60	Sable limoneux	Loamy sand	< 60	>0 – 60	3
LMS	Limon moyen sableux	Medium silt loam	> 60	198 – 330	1
LMS60	Limon moyen sableux	Medium silt loam	< 60	>0 – 99	3*
LS	Limon sableux	Sandy loam	> 60	186 – 310	1
LS60	Limon sableux	Sandy loam	< 60	>0 – 93	3*
LSA	Limon sablo-argileux	Sandy clay loam	> 60	198 – 330	1
LSA60	Limon sablo-argileux	Sandy clay loam	< 60	>0 – 99	3*
LAS	Limon argilo sableux	Silt sandy loam	> 60	180 – 360	1
LAS60	Limon argilo sableux	Silt sandy loam	< 60	>0 – 108	3*

[1)] Literal translation. Terms do not refer to the soil texture classification by the United States Department of Agriculture (USDA n. d.) ; [2)] Data provided by SMEGA; [3)] Source: Chambre d'Agriculture de l'Aisne 2007; * = the value could also be 2, because the range of possible *RZAWC* values overlaps both with risk class 2 and risk class 3. Risk class 3 was chosen because the overlap with this class is larger.

Figure 7 shows the risk map of the parameter *soil*. In the Ic, risk classes 1 and 3 exist to similar shares (~49 % and ~51 %, respectively), while risk class 2 is not present (Table 8). In general, it can be concluded that the northern parts of the Ic catchment have a higher risk for leaching of NO_3^- into the groundwater than the southern parts. The two dominating soil texture types (limon moyen sableux and limon argilo-sableux) in the catchment generally have a low risk of NO_3^- export, both regarding surface and subsurface flow, since they have high silt contents. The differences between particular parts of the catchment are mainly due to differences in soil depth. Almost all areas that belong to risk class 3 consist of shallow soils (below 60 cm), with the exception of soil class ‘SL’ (Table 7). The northern part of the catchment comprises shallow soils below 60 cm, which leads to high risk class mainly in this area. The soil depth map is shown in Figure 8.

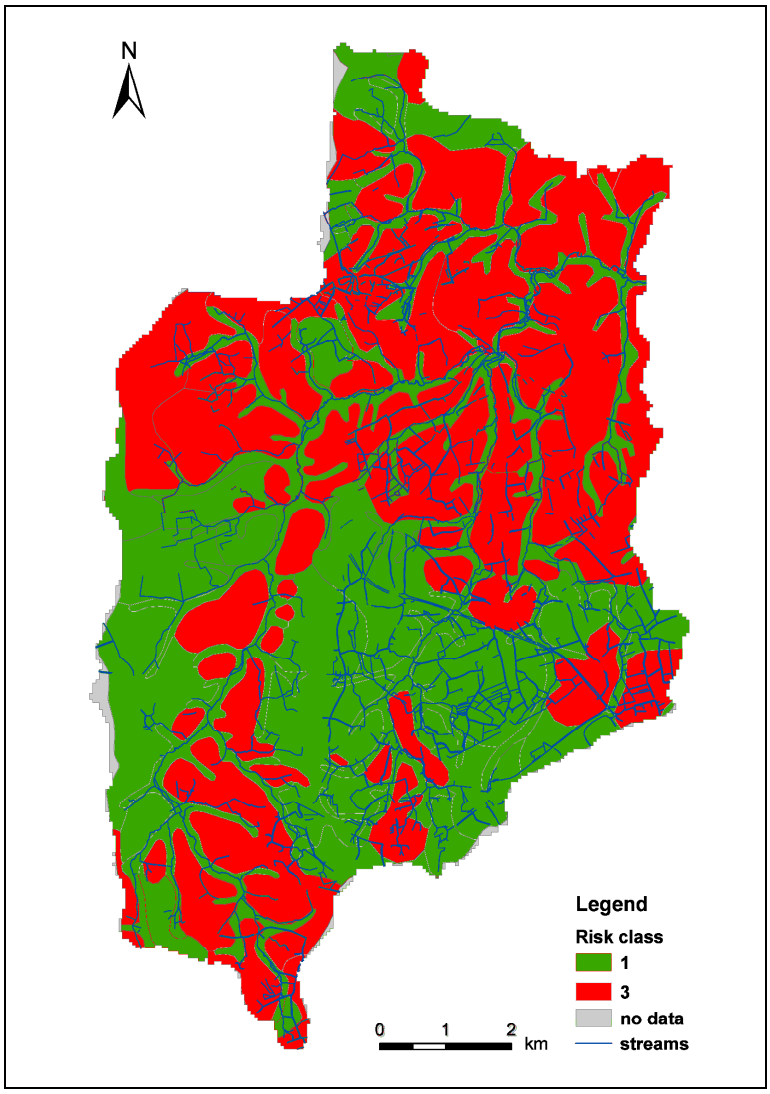

Figure 7. Risk map of the parameter *soil*.

Table 8. Percentages of risk classes for the parameter *soil*.

Risk class	Percentage of total area [%]
1	48.8
2	0
3	51.2

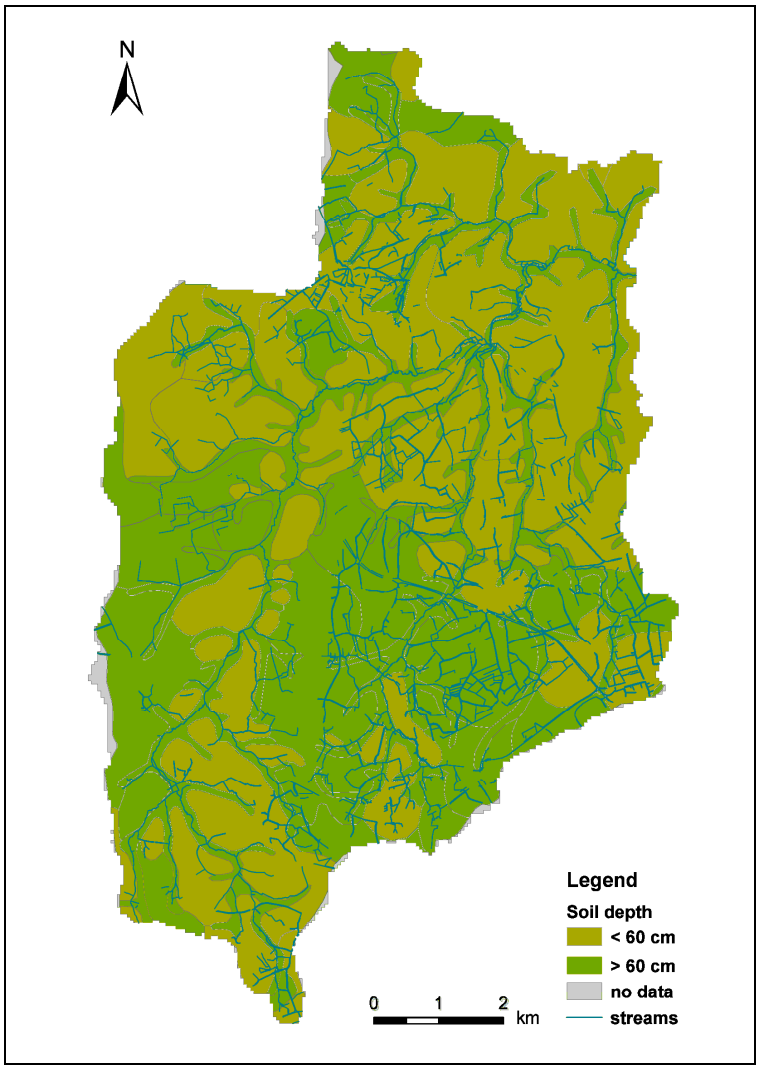

Figure 8. Soil depth map (data provided by SMEGA).

Discussion of the parameter soil

NO_3^- leaching from soil is difficult to represent with easily available data. In order to fulfil the scope of this work, the determination of *RZAWC* was reduced to the information of soil texture while land use and groundwater influence are omitted. Effective density is considered medium.

It should be kept in mind that the risk classes are chosen according to the risk for NO_3^- leaching to groundwater. Risk for surface runoff is not represented by this parameter. High risk in this layer can mean low risk regarding surface runoff.

The application to the Ic indicates that information on soil depth can have significant impact on the results for catchments with large areas of shallow soils. If shallow soils are

present in a catchment, but information on soil depth is not available, the reliability of the results solely based on soil texture is questionable.

For the Ic catchment, the local 'Conseil Général' has provided 16 soil profiles within the catchment and the area close-by the watershed divide. The profiles do not all confirm the soil type stated in the soil map and in the data from SMEGA, which indicates that the soil map might not be very accurate. However, the catchment-wide available soil data were used in the present study due to the requirement of comprehensive data. The quality of the soil data could not be verified within this study.

3.3.3 Slope

Importance of parameter slope

Even though NO_3^- is predominantly transported in dissolved form via infiltration, particulate transport via surface runoff does also exist depending on catchment characteristics (Karr and Schlosser 1978; Jordan et al. 2004; Mayer *et al.* 2005). Moreover, organic N can be transported to rivers via erosion, where it is mineralized to NH_4^+ and oxidized to NO_3^- (e.g., Brunet *et al.* 2008). This is also underlined by the detailed study on the River Elbe, where surface runoff contributed between 1 and 7 % of total agricultural diffuse pollution on average, in different subcatchments (Arbeitsgemeinschaft für die Reinhaltung der Elbe 2001). In order to account for surface runoff it is reasonable to consider slope as a parameter. Note that soil was not included in the following risk class definition to avoid cancelling out of the groundwater and surface runoff parameter.

Definition of risk classes

First, it was considered to use the empirical 'Universal Soil Loss Equation' (USLE) (Wishmeier and Smith 1965) to account for NO_3^- export by surface runoff, but the USLE is very detailed and the data requirements are high. A modified version of the USLE ('modified USLE') includes soil, distance to water and land use as well as slope (Sivertun *et al.* 1988):

$$P = K * S * W * U \text{, [-]} \qquad (4)$$

where P = product map; K = soil factor map; S = slope factor map; W = watercourse factor map and U = land use factor map.

Since *W* and *U* are already considered in other parameters of the present study it was decided to use slope as a single parameter to represent surface runoff. Soil factor *K* is increasing with decreasing permeability. The inclusion of *K* would partly cancel out the effect of the parameter *soil*, which assesses the risk of NO_3^- leaching. As a result, *K* was neglected and only slope was considered to assess the risk of surface runoff.

As in the modified USLE (Sivertun *et al.* 1988), the slope parameter refers only to slope steepness. Slope length was not considered, because soil loss increases much faster with slope steepness than with slope length (Scheffer 1989, p. 470). Furthermore, the determination of slope length involves complex calculations (Hickey 2000) and it was decided not to include this factor in order to keep calculations simple.

Nearing (1997) published a detailed review of studies on the relation between slope steepness and erosion. Based on the results of those studies he developed the following empirical equation for the slope steepness factor *S* of the USLE:

$$S = -1.5 + \frac{17}{1 + e^{2.3 - 6.1 \sin\theta}}\ , [-] \qquad (5)$$

where *S* = slope steepness factor [-] and θ = slope angle [°]. According to Equation 5 the maximum value for *S* (S_{max}) is 15.1. For the purpose of this study S_{max} was evenly divided into three classes (class limits at *S* = 5 and *S* = 10) and the corresponding angles were determined by solving Equation 5 for θ:

$$\theta = \arcsin\left(\frac{\ln\left(\frac{17}{S + 1.5} - 1\right) - 2.3}{-6.1}\right) \qquad (6)$$

Equation 5 is plotted in Figure 9. The red arrows depict the division of slope steepness factor *S* into three equidistant classes and the black arrows show the according values for θ. The resulting slope angles θ were used for the risk classification in this study.

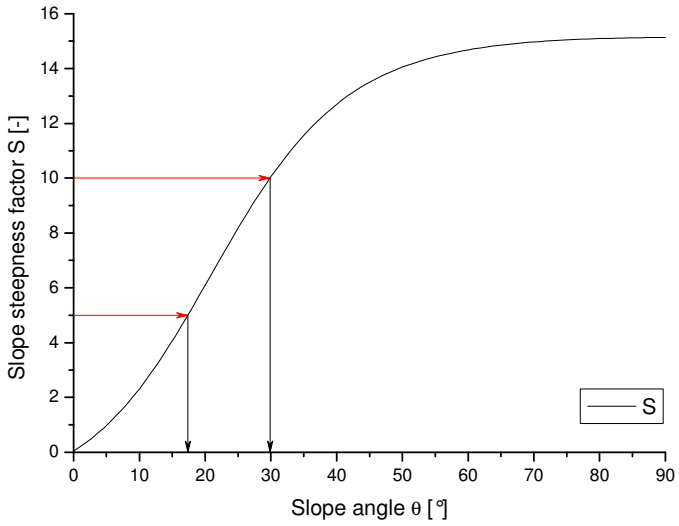

Figure 9. Plot of Equation 5: USLE slope factor S as a function of slope. Black arrows show the limits for risk classes.

Table 9. Risk classes for the parameter *slope*.

Risk class	Slope [°]	Slope [%]
1	0 – 17.4	0 – 31.3
2	17.5 – 29.9	31.4 – 57.5
3	30 – 90	57.8 - ∞

Data requirements

(a) Requirements: DEM or slope map

(b) Additional data: no

Application to the Ic

The DEM 50 was used to generate slope values for the Ic catchment. The results were classified according to the risk classes determined in 4.3.1 (Table 9).The flow chart on the steps performed can be found in the appendix (B 4.)

Figure 10 shows the resulting risk map. According to the risk classification described in 4.3.1, the Ic catchment does not comprise high risk areas (risk class 3) for erosion due to low slopes (Table 10). Even medium risk class areas are rare with 0.2 % of the whole

catchment. The maximum slope in the catchment of ~22 ° is at lower end of the medium risk class.

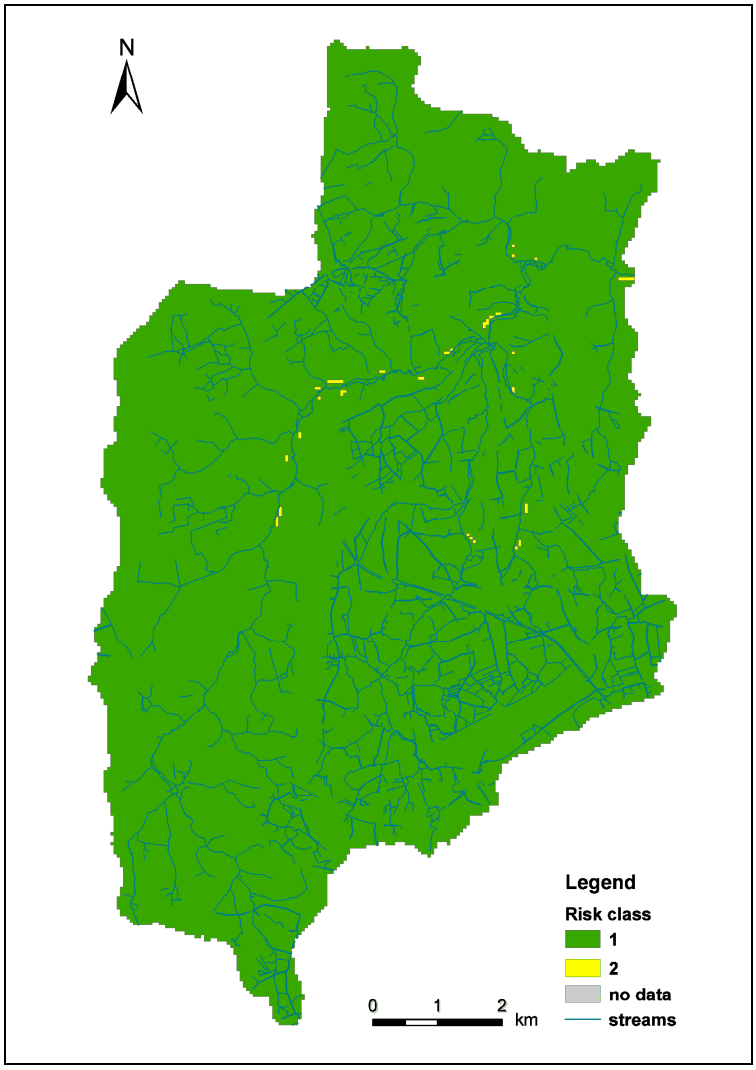

Figure 10. Risk map of the parameter *slope.*

Table 10. Percentages of risk classes for the parameter *slope.*

Risk class	Percentage of total area [%]
1	99.8
2	0.2
3	0

Discussion of the parameter slope

While the equidistant slope steepness classification according to Nearing (1997) is reasonable and physically-based regarding the full range of possible slopes (0 – 90°), the ranking may have to be reviewed for catchments with plain topography. As indicated in Figure 9, erosion is even occurring below slopes of 17.4 °.

The modified USLE defines the highest risk class for slopes >14% (>8°) (Sivertun and Prange 2003). This shows that the chosen equal distribution of this study might underestimate the risk in a catchment since 14% is within the lowest risk class chosen in this work. In the case of the Ic about 6% of the catchment area show slopes above 14% and consequently at least some erosion can be expected.

Given the monotonous nature of the function in Figure 9, one might consider to limit the ranking to the range of values found in a specific catchment (e.g., 0 to 22° for the Ic). Nevertheless, the global ranking was chosen for the purpose of transferability and comparability of the different parameters.

3.3.4 Riparian buffer strips

Importance of the parameter buffer strips

An important factor influencing how much NO_3^- reaches the surface waters is the land use within a close distance to the surface waters. If the land around surface waters is naturally vegetated (e.g., forests), i.e., if a buffer strip exists, the risk that nutrients reach the surface waters is lower (Mayer *et al.* 2005).

Riparian forests effectively inhibit NO_3^- and other pollutant transport to rivers (e.g., Maillard and Pinheiro Santos 2008; Basnyat *et al.* 2000; Peterjohn and Correll 1984; Jordan et al. 1993). The root zone provides an environment that favors microbial denitrification because of slight changes of the borders between the oxic and the anoxic zones. Furthermore nutrients are taken up for biomass growth (e.g., Basnyat *et al.* 2000; Wenger 1999).

Basnyat *et al.* (2000) showed that the correlation between land use and water quality has a higher determination coefficient (R^2) if only a buffer zone around the streams is considered than if the whole catchment is included in the analysis. Maillard and Pinheiro Santos (2008) further emphasize the importance of riparian zones for nutrient removal and ecosystem health.

In the following, the terms *riparian buffer strips* and *buffers* will be used synonymously.

Definition of risk classes

The parameter *riparian buffer strips* in this study assesses which land use type is passed by water from any point in the catchment immediately before entering the streams.

For the inclusion of the attenuating effect of buffer strips, a buffer strip width must be decided on. The removal effectiveness per width of the strip found in different studies varied to a great extent, but they all showed that forest or grass buffers around rivers decreased NO_3^- input significantly (Mayer *et al.* 2005).

Mayer *et al.* (2005) reviewed about 40 studies on the effect of buffer width on NO_3^- removal effectiveness and developed a non-linear regression model from those studies. Forest buffer removal effectiveness was high at all widths, i.e., no relationship with the width was found. For other buffer types width was a significant parameter influencing the effectiveness; however, other parameters, such as flow path, vegetation type and depth of root zone also affect N removal effectiveness. According to the model by Mayer *et al.* (2005) the following NO_3^- removal efficiencies were found: 50% at 3 m; 75% at 28 m; 90% at 112 m. According to Wenger (1999) a buffer should be at least 15 m in order to remove N effectively. The wider the buffer, the more denitrification sites are likely to be present. Welsch (1991) recommends a 29 m wide buffer strip around streams, while the standard in North Carolina (USA) suggests a 15 m wide buffer (Gilliam *et al.* 1997).

The wide range of observed results does not allow a definite decision on the buffer width. In the following, a width of 25 m was chosen, which is in the range of the above recommendations and is likely to lead to a significant removal of NO_3^- according to Mayer *et al.* (2005).

Regarding land use of the buffer strip, a forested buffer was found to remove NO_3^- most effectively, followed by a grass-covered riparian buffer (Mayer *et al.* 2005). A grassland buffer even has a certain retaining effect, if it is agriculturally used (fertilized or grazed) (Di and Cameron 2002). The highest risk of NO_3^- input occurs when no buffer zone is present, i.e., when agricultural cropland extends all the way to the river. Accordingly, the risk classes chosen for *riparian buffer strips* correspond to the risk classes created for the parameter *land use* (Table 11).

For the designation of the risk classes on all land surfaces, the following steps have to be performed (for a more detailed flow chart describing the application on the Ic catchment see appendix B 5.):

(1) Creation of the 25 m buffer around the stream network with GIS.

(2) Clipping the land use layer with the buffer layer.

(3) Calculation of watersheds using the 'watershed' function (Hydrology Toolset) of the Spatial Analyst extension in ArcGIS (Environmental Systems Research Institute 2005b). The layer resulting from (2) is used as 'pour point' data.

The result of these steps is a map which shows the risk class for each point on the land surfaces depending on the land use type they drain through immediately before entering the streams (Table 11). For instance, if water from an agricultural field flows through a forested strip before entering a stream, risk class 1 is assigned and vice versa, if water from a forested area flows through a cropland strip before entering the stream, risk class 3 is assigned. The buffer strips themselves are assigned the risk class which corresponds to their land use.

If possible, information on streams should be as precise as possible; including artificial (drainage) ditches, since their presence strongly influences the designation of risk areas.

Table 11. Risk classes for the parameter *riparian buffer strips*.

Risk class	Riparian buffer type
1	Unfertilized areas (e.g., forests)
2	Other fertilized areas (e.g., grasslands)
3	None (cropland)

Data requirements

(a) Requirements: DEM; stream network (from DEM or available maps); land use (of riparian buffers)

(b) Additional data: stream data can be refined via aerial photographs to include artificial ditches or even tile drains. However, it has to be noted that locations of tile drains are generally poorly mapped in most catchments (either no map or information at a too wide scale, e.g. communal level in France).

Application to the Ic

The watersheds are created as described above for the 25 m strip surrounding the stream network of the Ic. The stream network used is not created from the DEM 50, but had been digitized from aerial photographs. It was decided to use this digitized stream network since it contains information on small ditches present in some parts of the catchment, which are not reflected in the DEM 50. The inclusion of ditches is important,

since they drain a significant part of the catchment. Moreover, they are typically surrounded by agricultural cropland and therefore have a great impact on the transport of NO_3^- into the connected streams.

Figure 11 shows the risk map of the parameter *riparian buffer strips* for the Ic. The saturated colors show the 25 m buffer around the streams, which served as pour points in the GIS watershed tool. The transparent colors on the remaining areas show the calculated watersheds with their assigned risk classes depending on the connected riparian buffer type. Note that saturated and transparent colors are only shown for the sake of clarity, but are treated the same in the analysis (e.g., saturated and transparent red correspond both to risk class 3).

The risk map shows an enhanced risk in the south-eastern areas of the catchment, which are dominated by a dense grid of drainage ditches. Many of the areas around the main rivers in almost all subcatchments except for Ville Serho have a lower risk because the rivers are surrounded by a forested buffer. The map shows clearly how important the role of the dense network of ditches in the south-east is, since they cause the designation of many high risk areas.

Table 12 shows that ~23 % of the area of the Ic catchment is protected by a forested riparian buffer, while the water from almost half of the catchment does not at all pass through a riparian buffer strip.

Table 12. Percentages of risk classes for the parameter *riparian buffer strips*.

Risk class	Percentage of total area [%]
1	22.5
2	27.6
3	46.8

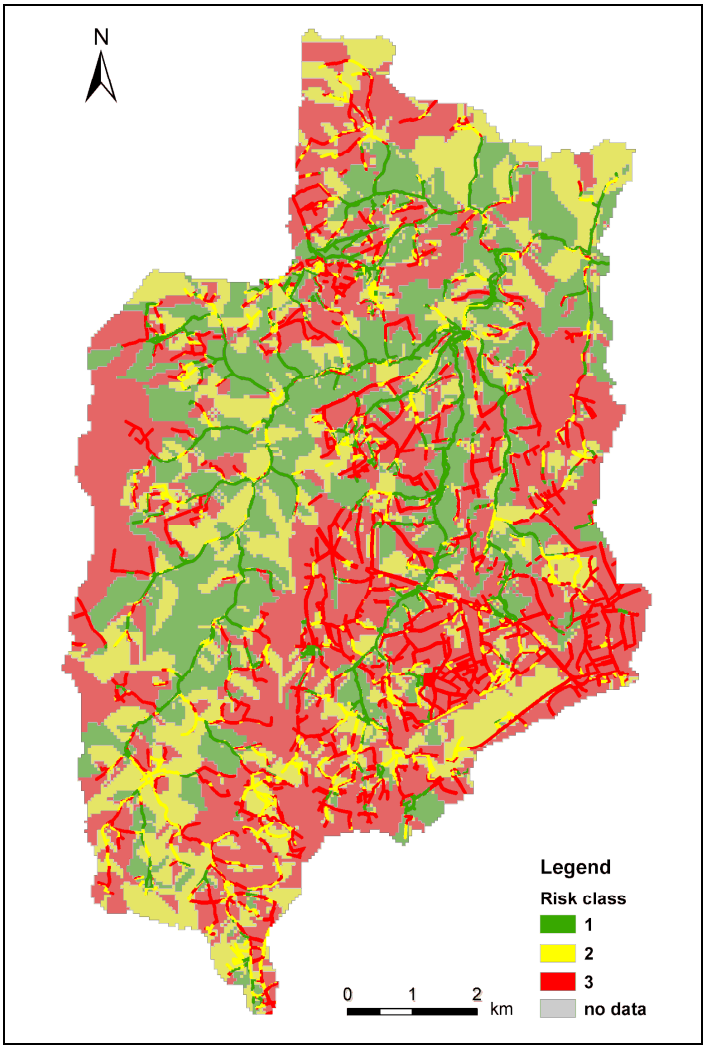

Figure 11. Risk map of the parameter *riparian buffer strips.* Note that the saturated and the transparent version of a color stand for the same risk class.

Discussion of the parameter riparian buffer strips

The quality of the result for this layer is very much dependent on the resolution of the DEM and the quality of the land use data as well as the stream data.

Visits in the Ic catchment suggest that the artificial ditches are unevenly recorded throughout the catchment, e.g., in the subcatchment Ic Amont some ditches have been found which are not depicted in the stream network map (A. Matzinger, personal communication). This raises the question of the quality of the stream data in the Ic catchment. However, the stream network from aerial photographs was chosen, because it still reflects more surface water bodies in the Ic than the stream network derived from the DEM 50.

3.3.5 Distance to surface waters

Importance of the parameter distance to surface waters

Many studies assessing pollution risks include the parameter *distance to surface waters* (e.g., Maillard and Pinheiro Santos 2008; Basnyat *et al.* 2000; Sivertun and Prange 2003). The modified USLE (Sivertun *et al.* 1988), which assesses the erosion risk in an area, includes the distance to surface waters in the so-called 'watercourse factor map'.

As mentioned in 3.3.4, Basnyat *et al.* (2000) found a better correlation between land use and water quality if only land use within a certain distance from the streams was considered instead of the land use in the whole catchment. Their findings show that the distance of a point to the river is relevant to its effect on the NO_3^- concentration in the water.

King *et al.* (2005) studied the correlation between distance-weighted cropland and NO_3^--N concentrations in the Costal Plain of Maryland (USA). They found that distance-weighting of the percentage of cropland leads to better predictions of the NO_3^--N concentrations in the stream.

All studies cited above reveal that it is reasonable taking distance into account. In the following the terms *distance to surface waters* and *distance* will be used synonymously.

Definition of risk classes

The definition of risk classes for the parameter *distance to surface waters* is based on the modified USLE (Sivertun *et al.* 1988). The modified USLE includes a 'watercourse factor map', which corresponds to the parameter *distance to surface waters* of this study. Sivertun and Prange (2003) state that the 'modified USLE' refers to pollution in general. However, it should be mentioned that both the 'USLE' and the 'modified USLE' generally apply to erosion and reflect therefore mainly the transport of substances in particulate form. Thus, phosphorus and particulate N pollution is better represented by this approach than dissolved NO_3^- load. No information could be found on the correlation between distance to surface waters and proportion of NO_3^- reaching the watercourses. Nevertheless, it was assumed that the probability of any substance to reach the watercourse is increased at close distance, both for surface runoff and groundwater passage. As a result, the 'watercourse factor map' of the modified USLE was used for the definition of risk classes in the present study.

Sivertun and Prange (2003) show the percentages of pollution load that reaches the stream from different distances. They consider the four classes from the modified USLE

(< 50 m, 50 – 200 m, 200 – 1000 m, > 1000 m). For the present approach three risk classes are required to allow direct comparability. Therefore the last two classes of the modified USLE were combined while the other two were adopted directly.

The above classification is corroborated by a study of King *et al.* (2005) who performed distance-weighting of land cover percentages and classified their catchment into <30 m, 31 - 100 m, 101 - 250 m, 251 – 500, 501 – 1000 and > 1000 m buffers. Reducing the number of classes to three could result in the following classification: <30 m, 31 – 250 m and > 250 m, which is in the same order of magnitude as the chosen classification based on the modified USLE.

Most studies that include distance or riparian buffers use the 'buffer function' of ArcGIS, which is based on the 'Euclidean distance' (e.g., Basnyat *et al.* 2000; Maillard and Pinheiro Santos 2008) or the 'Euclidean distance' function (e.g., King *et al.* 2005). Similar to those approaches, the 'Euclidean distance' function is applied here for the display of the risk classes.

If possible, artificial ditches should be included in the stream data since their presence greatly influences the proximity of an area to the next surface water.

Table 13. Risk classes for the parameter *distance to surface waters*.

Risk class	Distance
1	> 200 m
2	50 – 200 m
3	0 – 50 m

Data requirements

(a) Requirements: stream network (from DEM or available maps)

(b) Additional data: stream data can be refined via aerial photographs to include artificial ditches or even tile drains.

Application to the Ic

The stream network used is the same as for the parameter *riparian buffer strips* and consists of digitized streams from aerial photographs. These data include ditches and small streams that cannot be distinguished in a stream network generated from the DEM 50 and was therefore preferred for the purpose of this study.

The resulting risk map for the parameter *distance to surface waters* (Figure 12) shows that many of the risk class 3 areas are located in the south-eastern parts of the catchment, where a tighter stream network (mainly due to ditches) is present. About 38 % of the catchment area are classified risk class 3 (Table 14). The 16 % risk class 1 areas are mainly in the north and in the west of the catchment (Figure 12; Table 14).

The flow chart describing the creation of the risk map for the parameter distance to surface waters can be found in the appendix (B 6.).

Table 14 Percentages of risk classes for the parameter *distance to surface waters*.

Risk class	Percentage of total area [%]
1	16.0
2	45.9
3	38.1

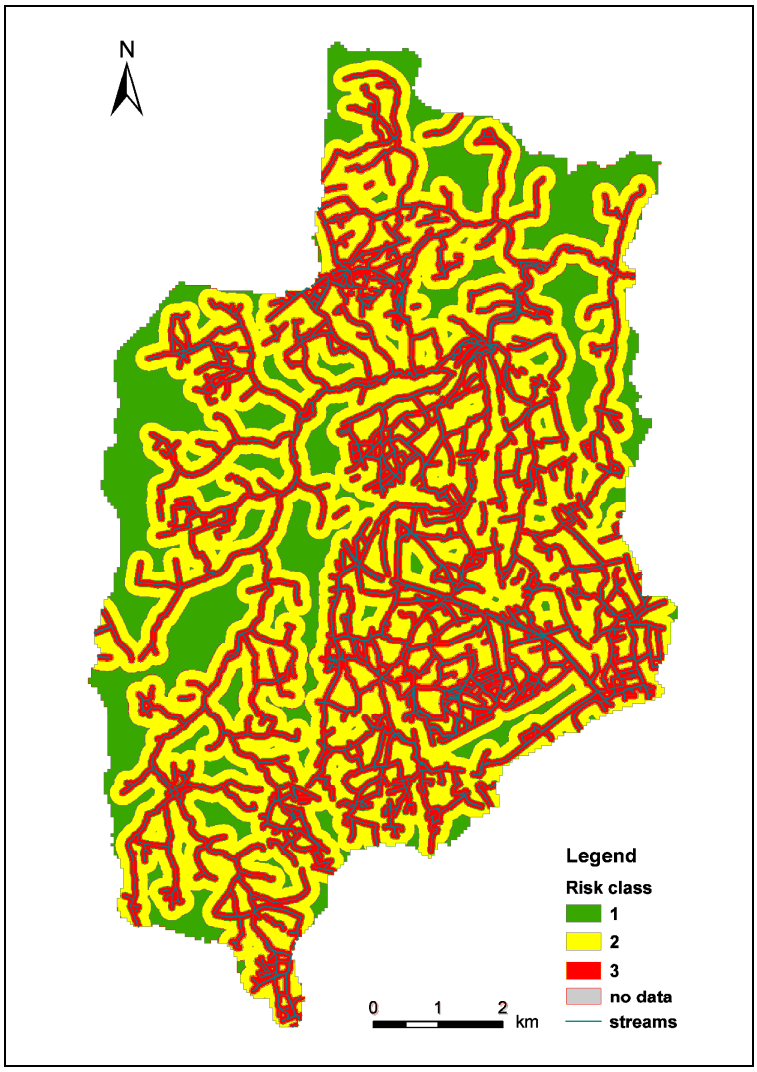

Figure 12. Risk map of the parameter *distance to surface waters*.

Discussion of the parameter distance to surface water

As mentioned above, ‘Euclidean distance’ was used for the designation of risk areas. This approach does not reflect the actual flow path from a certain point in the catchment to the surface water body. The actual flow path for every point in the catchment to the next surface water is difficult to determine because it depends on the transport processes (surface versus subsurface) which are presumably not known in a given catchment. Furthermore the DEM usually does not have the affordable precision for that problem. Thus, the actual flow path is not included in the study. Moreover, a function to calculate the actual flow path is not yet included in ArcGIS 9.1. Due to the technical restrictions there are inaccuracies in both Euclidean distance and flow path, so in order to keep the approach simple and generally applicable the 'Euclidean distance' function was chosen.

As previously mentioned in Chapter 3.3.4, visits in the Ic catchment have shown that not all ditches are covered by the stream network data. The quality of the stream network data has a great effect on the quality of the result of the parameter *distance to surface waters*.

3.4 Overlay of parameters

3.4.1 Method

The creation of the five thematic maps concerning the risk of NO_3^- export is followed by a combination of all layers. Technically the overlay is performed by combining the GIS layers of the parameters with the 'raster calculator' of the Spatial Analyst extension of ArcGIS (Environmental Systems Research Institute 2005b). By applying the overlay, the mean risk class for each cell is calculated according to the following equation:

$$RC = \frac{\sum_{i=1}^{n} x_i}{n} \text{ [-]}, \qquad (7)$$

RC = risk class n = number of layers x_i = layer i.

In the following, the term 'overlay' refers to the calculation of the mean risk class for each cell. The results of the following 'overlay' are float values from 1 to 3. In order to make the results comparable the values had to be allocated to low, medium and high risk classes. An equidistant distribution was chosen in order to reflect all classes to the same extent:

- Low risk class = 1.000 – 1.666
- Medium risk class = 1.667 – 2.333
- High risk class = 2.334 – 3.000

A classification using mathematically rounded values was discarded, because it results in an overrepresentation of risk class 2, which would be twice as wide as the other two classes, since values below 1 and above 3 cannot occur.

3.4.2 Application to the Ic

The overlay of the five individual parameters of the Ic catchment described in Chapter 3.4.1 has a leveling effect, so that most areas belong to risk class 2 (63.1 %). High risk areas (risk class 3) exist mainly in the south-east and in the east of the catchment

(17.6 %) while low risk areas (risk class 1) can be found along the main rivers (19.3 %) (Table 15; Figure 13).

In the following, the seven subcatchments are abbreviated with the names of the according monitoring stations (see Table 16).

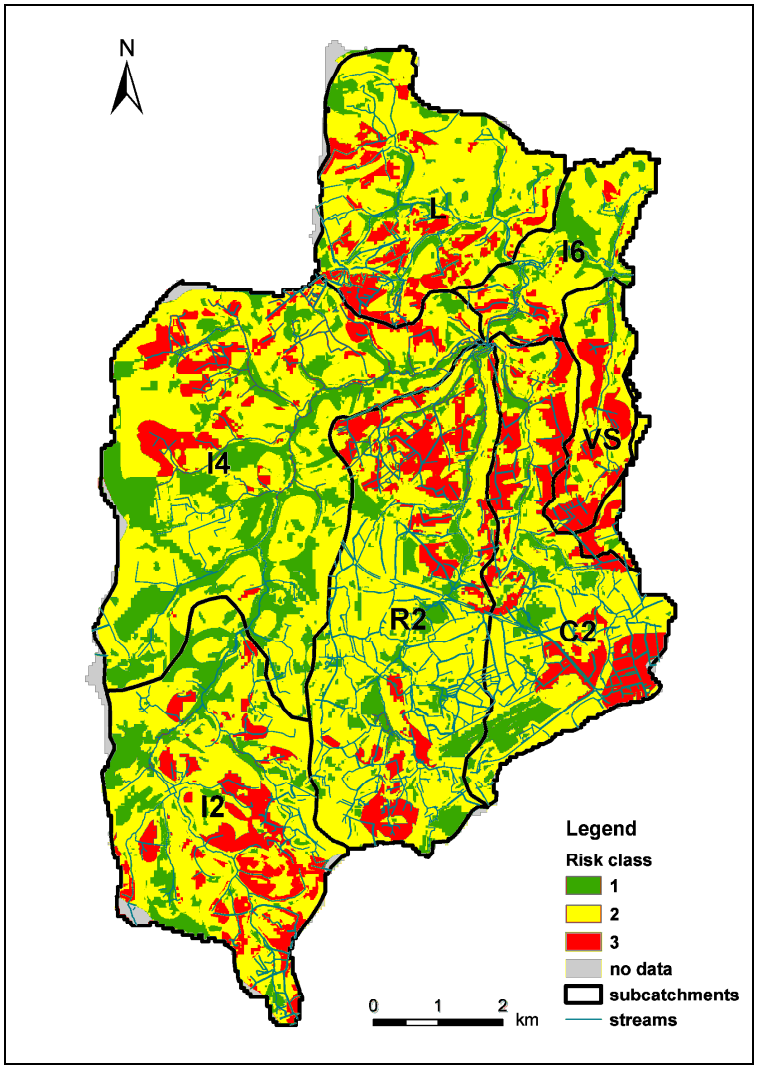

Figure 13. Overlay of five parameters (full overlay).

Table 15. Percentages of risk classes after the overlay.

Risk class	Percentage [%]
1	19.3
2	63.1
3	17.6

Chapter 4
Validation of the combined GIS approach

4.1 Comparison with nitrate loads

4.1.1 Comparison with measured nitrate loads

In order to validate the applied overlay, the results are compared with average NO_3^- loads obtained from ten years of monthly NO_3^- and discharge measurements at seven monitoring stations in the catchment. It is important to note that the calculation of NO_3^- loads based on monthly measurements can be subject to large (but unknown) errors, since fluctuations during storm events are not accounted for. Table 16 shows the ranking of the seven subcatchments in the order of decreasing mean risk classes. Although mean risk classes are all close to 2, a clear ranking is possible among the subcatchments. Corresponding NO_3^- loads can be found in the third column (compare also Figure 5 in Chapter 2). Ville Serho is the subcatchment with the highest load as well as with the highest mean risk class. However, the rankings of measured loads and mean risk classes do not coincide for all subcatchments. For instance, the subcatchment with the lowest mean risk class (Ic Centre) shows higher loads than some other catchments (Ic Littoral, Lantic) and almost as much as the catchment with the third highest mean risk class (Rodo). Measured loads are plotted against mean risk classes in Figure 14 for a more systematic overview. Correlation is not significant (p=0.057) concerning a confidence interval of 95 %. However, the general trend of higher mean risk class in a subcatchment with higher NO_3^- load can be shown. Yet, this does not apply to every data pair. Furthermore, it is not possible to receive reliable results on correlation from seven data points only.

Table 16. Mean risk classes and measured NO_3^- loads per subcatchment.

Sub-catchment	Monitoring station	Mean risk class [-]	NO_3^- load [kg NO_3^- N ha^{-1} yr^{-1}]
Ville Serho	VS1	2.1375	77.77
Camet	C2	2.0871	42.07
Rodo	R2	2.0248	33.58
Lantic	L2	2.0165	29.04
Ic Amont	I2	2.0008	45.30
Ic Littoral	I6	1.9163	15.86
Ic Centre	I4	1.8682	33.29

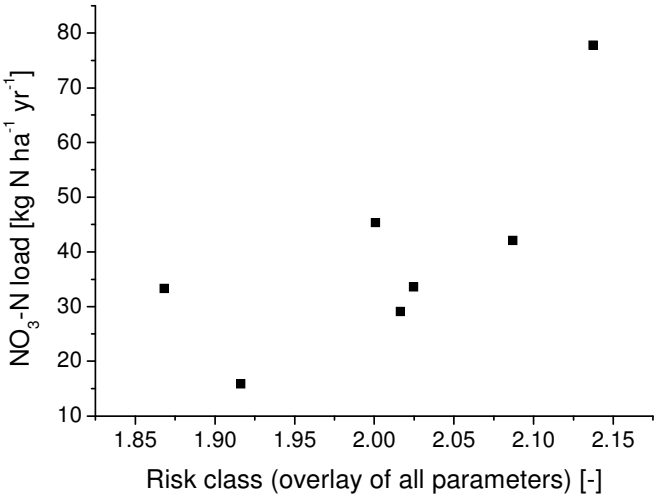

Figure 14. Measured NO_3^- loads plotted against mean risk class of subcatchments after full overlay.

4.1.2 Comparison with SWAT simulation

The SWAT analysis performed by Julich *et al.* (2009) simulated NO_3^--N loads for 32 subcatchments (SCs 1-32; Figure 15). The SWAT model was calibrated based on monthly discharge and NO_3^- loads. On the contrary to the present study the stream network used by Julich *et al.* (2009) was generated from the DEM50 and therefore artificial ditches were neglected. Data from the 16 soil profiles were included in the soil input data, which were neglected for the GIS approach of this work (see Chapter 3.3.2).

The visual comparison of Figure 15a and Figure 15b shows that the GIS results are fragmented. Both the approach of the present study and the SWAT analysis predict CSAs in the north-east (SCs 31, 27, 25 and 14) and in the south (SC 20) of the catchment. Major differences between the two approaches exist in the north-west where SWAT predicts low loads (SCs 2, 7 and 9), but the present study expects several CSAs. In other subcatchments (SCs 29 and 4 in the north or 23, 10 and 16 in the centre) SWAT predicts hotspots (highest and second highest SWAT classes), while those parts of the Ic catchment comprise mainly of areas classified in low and medium risk classes in the tested GIS approach.

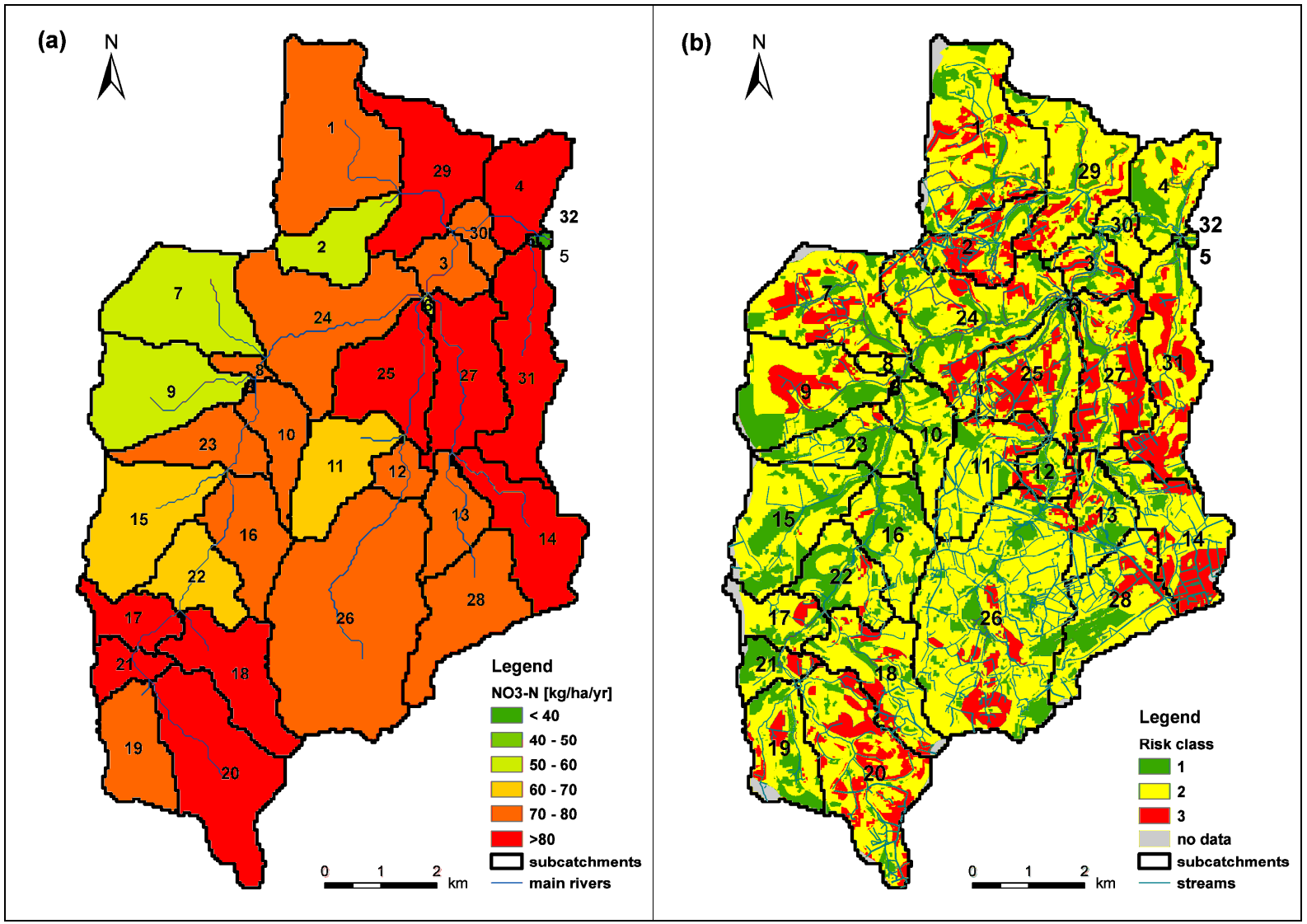

Figure 15. Comparison between the SWAT results and the results of the full overlay. (a) Result map of SWAT analysis (data provided by S. Julich). (b) Full overlay of five parameters in the 32 subcatchments of SWAT.

In order to compare the two approaches quantitatively, the mean risk classes of the GIS method in each of the 32 SCs are plotted against the NO_3^--N loads predicted by SWAT (Figure 15b). It was not attempted to assign the risk classes identified by the GIS approach to NO_3^--N loads predicted by SWAT, since a risk class definition cannot aim at predicting NO_3^--N loads.

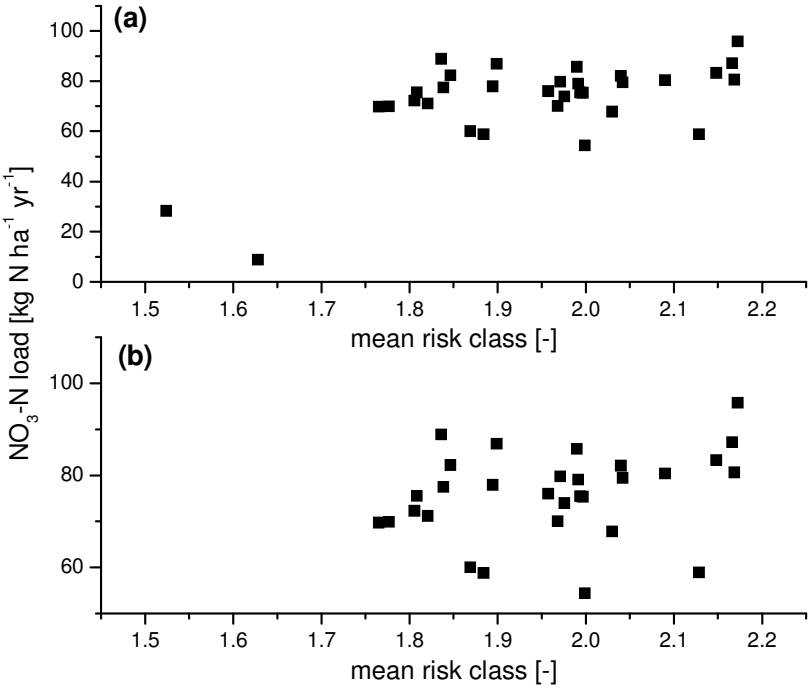

Figure 16. (a) Mean risk classes in the 32 SWAT subcatchments according to the tested GIS approach versus the predicted NO_3^--N loads by SWAT (SWAT data provided by S. Julich). (b) The same graph at different scale.

The two subcatchments classified of lowest risk are also predicted to have lowest NO_3^--N loads by SWAT (SCs 5 and 32). The SC with the highest risk class (20) also has the highest predicted NO_3^--N loads by SWAT. In between the extremes there is a weak tendency that higher risk classes also correspond to higher SWAT loads; however with a high scattering. For instance, the two SCs with the second and third highest SWAT NO_3^--N loads, respectively, have a quite low risk class (SCs 17 and 21). The two sets of data show a significant correlation ($R^2 = 0.38$ (linear model); p-value = $1.6 \cdot 10^{-4}$; Figure 16a). The two lowest points (SCs 5 and 32) are SCs with very small areas, but because of their accordance in both methods they have a very strong effect on the correlation. If they are excluded no more correlation is found ($R^2 = 0.08$ (linear model); p-value = 0.14; Figure 16b).

The detailed differences between the SWAT analysis and the tested GIS approach cannot be fully discussed here, since approaches are completely different. However, SCs 7 and 9, which show particularly high differences between the two approaches are discussed in some more detail. The comparably low loads in the SWAT approach are probably due to a significant share of forest (Figure 3). Correspondingly, the areas are also assigned low or moderate risk classes in the parameter land use of the GIS approach (Figure 6). The high risk class is mainly the result of the parameter *soil* (Figure 7) and to a lesser extent of the parameters *buffers* (Figure 11) and *distance* (Figure 12). The difference in applied soil data and soil evaluation of the two methods can thus partly explain the difference in the results. Additionally, the parameters *buffers* and *distance* are strongly influenced by the presence of drainage ditches, which occur in the two SCs to a moderate extent, but were neglected in the SWAT analysis (compare river networks in Figure 15a (SWAT) and Figure 15b (GIS)). This example indicates that a part of the deviations between the two approaches can be explained by different input data.

4.2 Sensitivity analysis

For the applicability of a similar GIS-based approach to catchments with varying data availability, it is important to know the sensitivity of the results to each parameter.

Visual comparison

The influence of each parameter can be tested by performing the overlay again but leaving out one parameter at a time. It can be depicted how omitting one parameter changes the resulting maps and the drawn conclusions. The result of this step contains five maps with four input parameters each. The maps are shown in Chapters 4.2.1 – 4.2.5 and first interpreted based on a visual comparison. In the following the previous overlay of five parameters is referred to as ‘full overlay’.

Comparison of subcatchment ranking

Apart from a visual comparison changes from neglecting one parameter can be assessed through the renewed ranking of mean risk classes for the seven subcatchments (Chapter 2).

NO_3^--N loads versus risk class of parameter

Finally, the parameter itself is considered. For each parameter measured NO_3^--N loads are plotted against the mean risk classes of the single parameters to get a rough idea of the correlation.

4.2.1 Land use

Visual comparison

Generally omitting *land use* leads to a general decrease in high risk classes; i.e., less predicted high risk areas and more predicted low risk areas. This can easily be understood, since *land use* contributes predominantly to the highest risk class (~64 % of the catchment, Table 3). However, the spatial distribution of high risk areas is very similar (Figure 17), which can be explained by the fairly homogeneous distribution of risk classes of the parameter *land use* over the whole catchment.

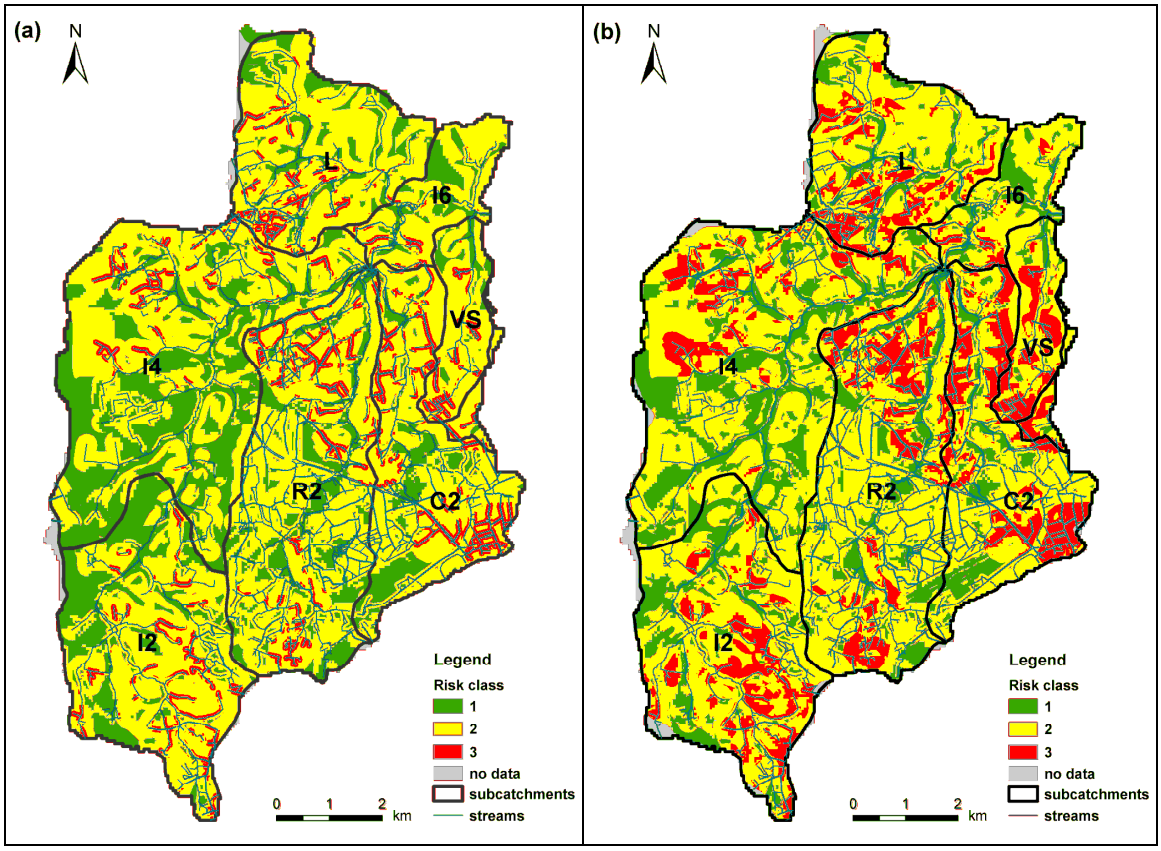

Figure 17. Overlay without parameter *land use* versus full overlay. (a) Overlay without parameter *land use.* (b) Full overlay of five parameters.

Comparison of subcatchment ranking

Table 17 shows that the mean risk classes in the seven subcatchments are all lower when the parameter *land use* is omitted. Compared to the ranking of the five layers, the ranking of the subcatchments does not change to a great extent; only ranks 3 and 4 are switched when *land use* is not included in the overlay. As already expected from visual comparison, the overlay without the parameter *land use* leads to very similar conclusions as the full overlay.

Table 17. Ranking of subcatchments after overlay without parameter *land use* versus full overlay.

Subcatchment	Without *land use*	Rank	Full overlay	Rank
Ville Serho	2.0307	1	2.1375	1
Camet	1.9716	2	2.0871	2
Rodo	1.8958	4*	2.0248	3
Lantic	1.9131	3*	2.0165	4
Ic Amont	1.8586	5	2.0008	5
Ic Littoral	1.8335	6	1.9163	6
Ic Centre	1.7476	7	1.8682	7

* rank differs from the one of the full overlay.

NO_3^--N loads versus risk class of parameter land use

Figure 18 shows the NO_3^--N loads plotted against the mean risk classes of the parameter *land use* in each subcatchment. A significant correlation could not be found ($R^2 = 0.505$ (linear model); $p = 0.07$). A reason might be that the relationship seems to be not linear but exponential.

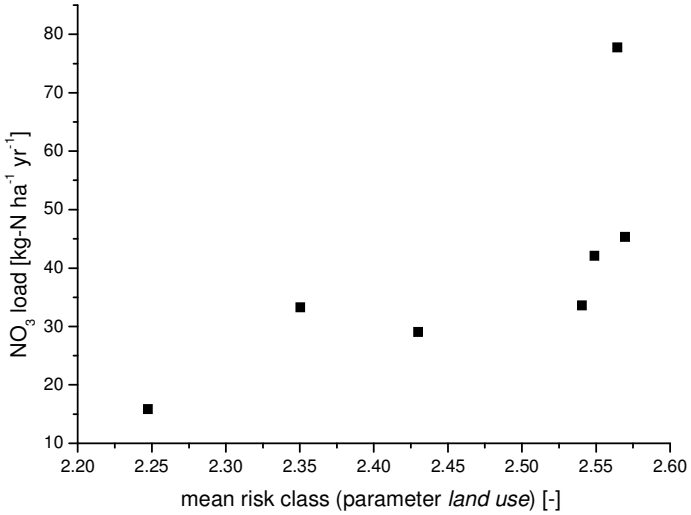

Figure 18. Measured NO_3^--N loads plotted against the mean risk classes of the parameter *land use*.

4.2.2 Soil

Visual comparison

The difference between the full overlay and the one without the parameter *soil* is noticeable. The CSAs in the west are smaller and appear more scattered further south in Figure 19a compared with Figure 19b. In contrast, in the south-west, especially along the ditches, the risk map without *soil* identifies more high risk areas than the one including all parameters. Obviously, the spatial distribution of high risk areas in the soil risk map (mainly in the north; Figure 7) has a high impact on the result of the full overlay, where the emphasis of high risk areas is mainly in the same regions as in the soil map (Figure 19b).

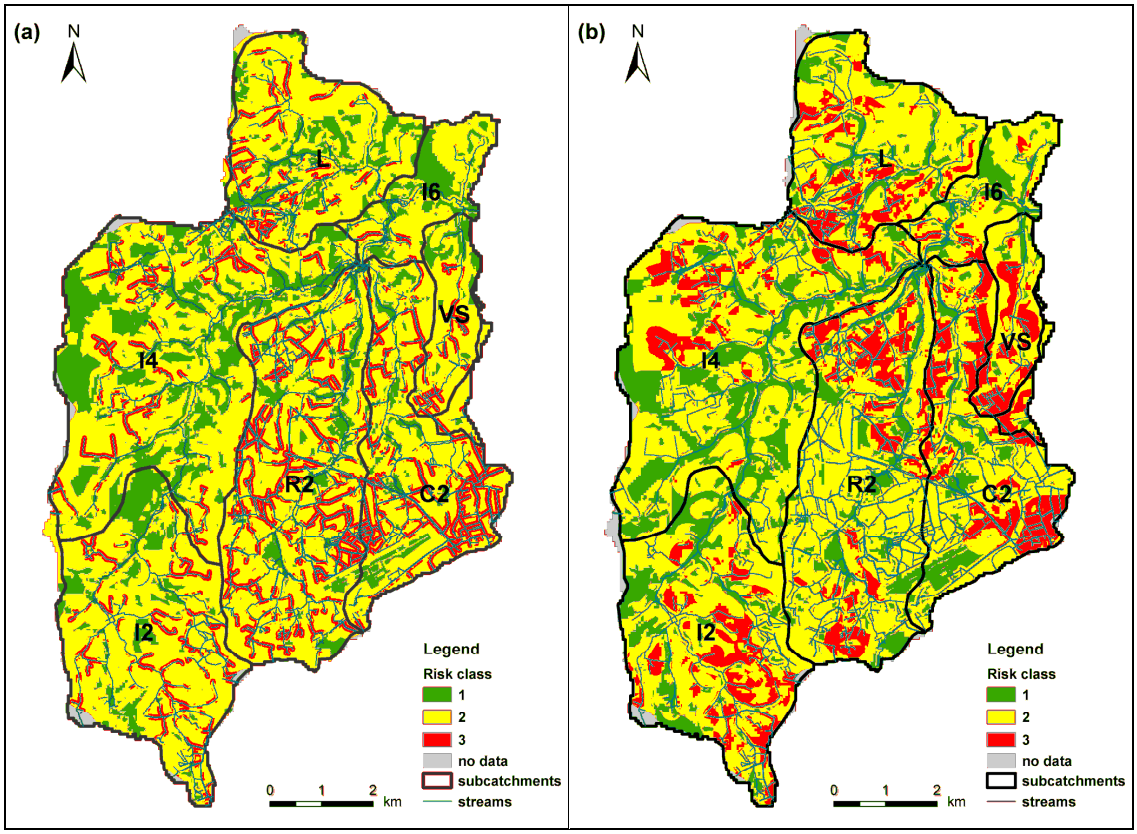

Figure 19. Overlay without parameter *soil* versus full overlay. (a) Overlay without parameter *soil.* (b) Full overlay of five parameters.

Comparison of subcatchment ranking

The order of mean risk classes in the subcatchments is very different in the overlay without the parameter *soil* compared to the full overlay (Table 18). In the full overlay Ville Serho has the highest mean risk class, followed by Camet and Rodo. In the overlay without *soil* Camet has the highest mean risk class, followed by Rodo and Ville Serho.

Even within those subcatchments, differences can be observed, e.g., in Camet in the full overlay the high risk areas are mainly in the northern parts of the subcatchment, while in the overlay without *soil* the high risk areas are further south in the subcatchment. In the map (Figure 19a) it can be seen that high risk areas are present mainly in the southern parts of Camet and Rodo when the parameter soil is omitted.

Due to the differences observed, omitting the parameter *soil* might lead to different conclusions, e.g., regarding the placing of mitigation zones.

Table 18. Ranking of subcatchments after overlay without parameter *soil* versus full overlay.

Subcatchment	Without *soil*	Rank	Full overlay	Rank
Ville Serho	2.0196	3*	2.1375	1
Camet	2.1150	1*	2.0871	2
Rodo	2.1076	2*	2.0248	3
Lantic	1.9556	5*	2.0165	4
Ic Amont	1.9910	4*	2.0008	5
Ic Littoral	1.7525	7*	1.9163	6
Ic Centre	1.8427	6*	1.8682	7

* rank differs from the one of the full overlay.

NO_3^--N loads versus risk class of parameter soil

Figure 18 shows the NO_3^--N loads plotted against the mean risk classes of the parameter *soil* in each subcatchment. A considerable correlation cannot be found due to the scattered data (R^2 = 0.05 (linear model); p-value = 0.6). A possible explanation might be that the parameter *soil* reflects only risk resulting from NO_3^- leakage to groundwater. Governing export processes differ between the subcatchments (see Chapter 2), so some catchments may be reflected better by the parameter *soil* than others. For instance, groundwater influence can be assumed to be higher in catchments with increased concentration at low discharges. However, if the two subcatchments which seem to be influenced by groundwater (unpublished data from KWB) are omitted, the correlation does not improve. This could be due to the fact that the measured NO_3^--N loads do not

include measurements at high discharges. Furthermore household effluents in the area could have an impact on NO_3^--N loads at low discharges.

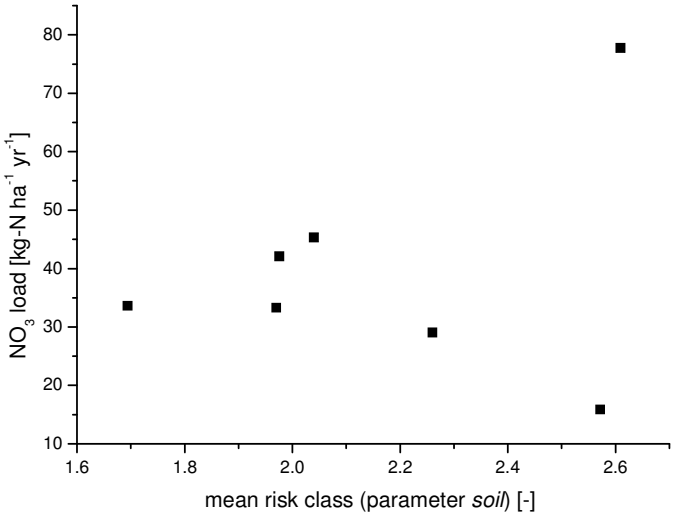

Figure 20. Measured NO_3^--N loads plotted against the mean risk classes of the parameter *soil.*

4.2.3 Slope

Visual comparison

The parameter *slope* decreases the overlay results for the whole catchment, since it is very homogeneous and almost the whole catchment is classified of low risk regarding this parameter (99.8 % risk class 1, the rest risk class 2; Table 10). Disregarding this parameter results in an increase of high risk areas. However, the centers of the main high risk areas are located in the same areas (Figure 21). Thus, the inclusion of the parameter *slope* leads to a more focused representation of very high risk areas, namely the ones which are classified as risk class 3 despite the lowering effect of the parameter on all areas.

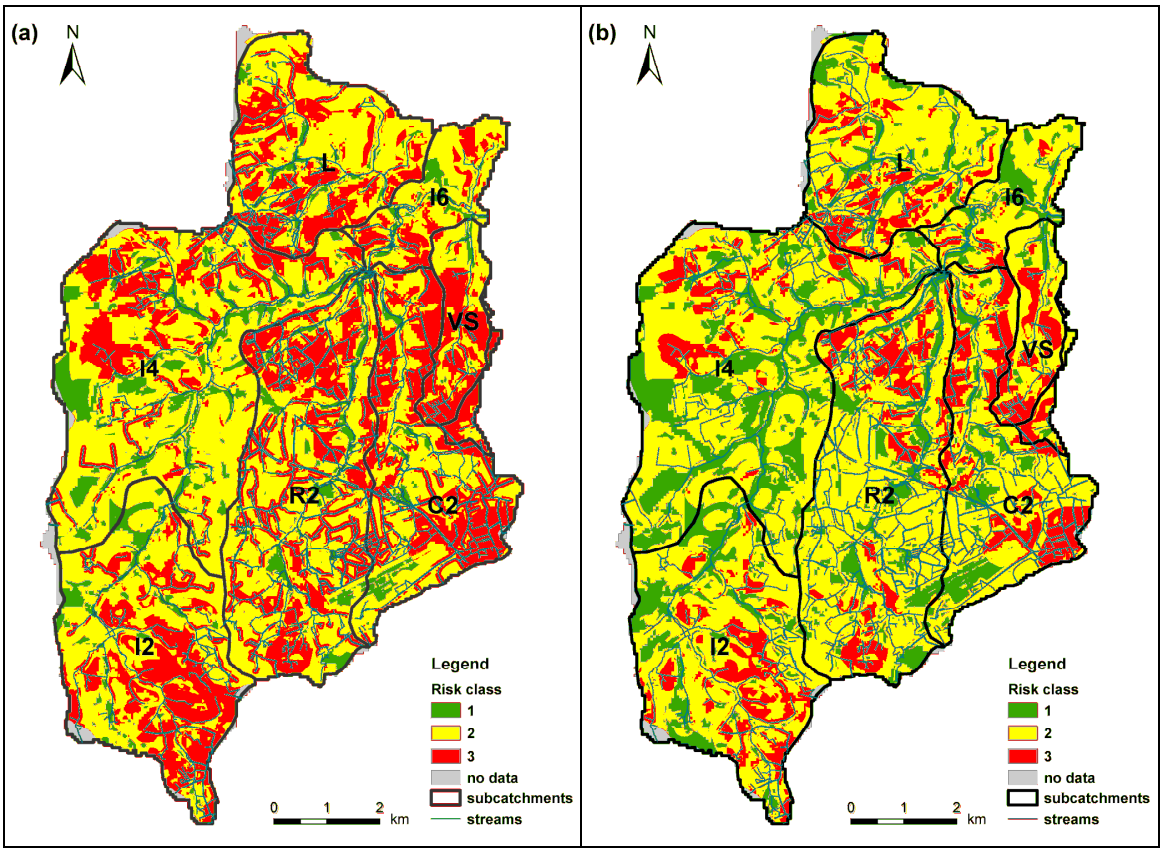

Figure 21. Overlay without parameter *slope* versus full overlay. (a) Overlay without parameter *slope.* (b) Full overlay of five parameters.

Comparison of subcatchment ranking

The ranking of subcatchments stays the same if the parameter slope is not included in the overlay, i.e., the drawn conclusions stay exactly the same. This is due to the homogeneous character of the parameter.

Table 19. Ranking of subcatchments after overlay without parameter *slope* versus full overlay.

Subcatchment	Without slope	Rank	Full overlay	Rank
Ville Serho	2.4219	1	2.1375	1
Camet	2.3584	2	2.0871	2
Rodo	2.2809	3	2.0248	3
Lantic	2.2705	4	2.0165	4
Ic Amont	2.2510	5	2.0008	5
Ic Littoral	2.1433	6	1.9163	6
Ic Centre	2.0845	7	1.8682	7

NO_3^--N loads versus risk class of parameter slope

Since the risk class of the parameter *slope* is low everywhere in the catchment, the range of the mean risk classes is rather small (compare values at the x-axis of Figure 22). Thus, the inversely proportional tendency in Figure 22 might be random. Moreover, *slope* and NO_3^--N loads do not correlate significantly (R^2 = 0.39 (linear model), p-value = 0.13).

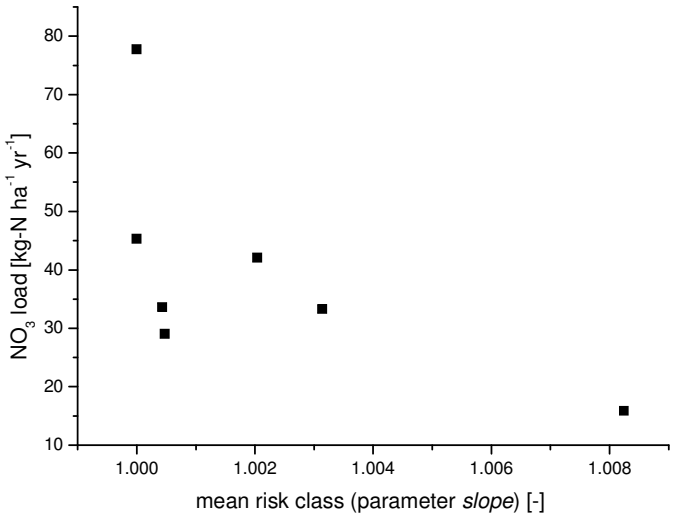

Figure 22. Measured NO_3^--N loads plotted against the mean risk classes of the parameter *slope*.

4.2.4 Riparian buffer strips

Visual comparison

Omitting the parameter *riparian buffer strips* leads to fewer CSAs than the overlay of all parameters (Figure 23). The identified CSAs are in the same regions as for the full overlay but more focused. The locations of the resulting CSAs are very similar to the ones in the overlay without *land use* (Figure 17). The largest difference is seen for the western part of the catchment, which gets a higher share of risk class 1. The reason is that some larger parts of non-fertilized areas in the western catchment are drained through agricultural cropland, which extends all the way to the river.

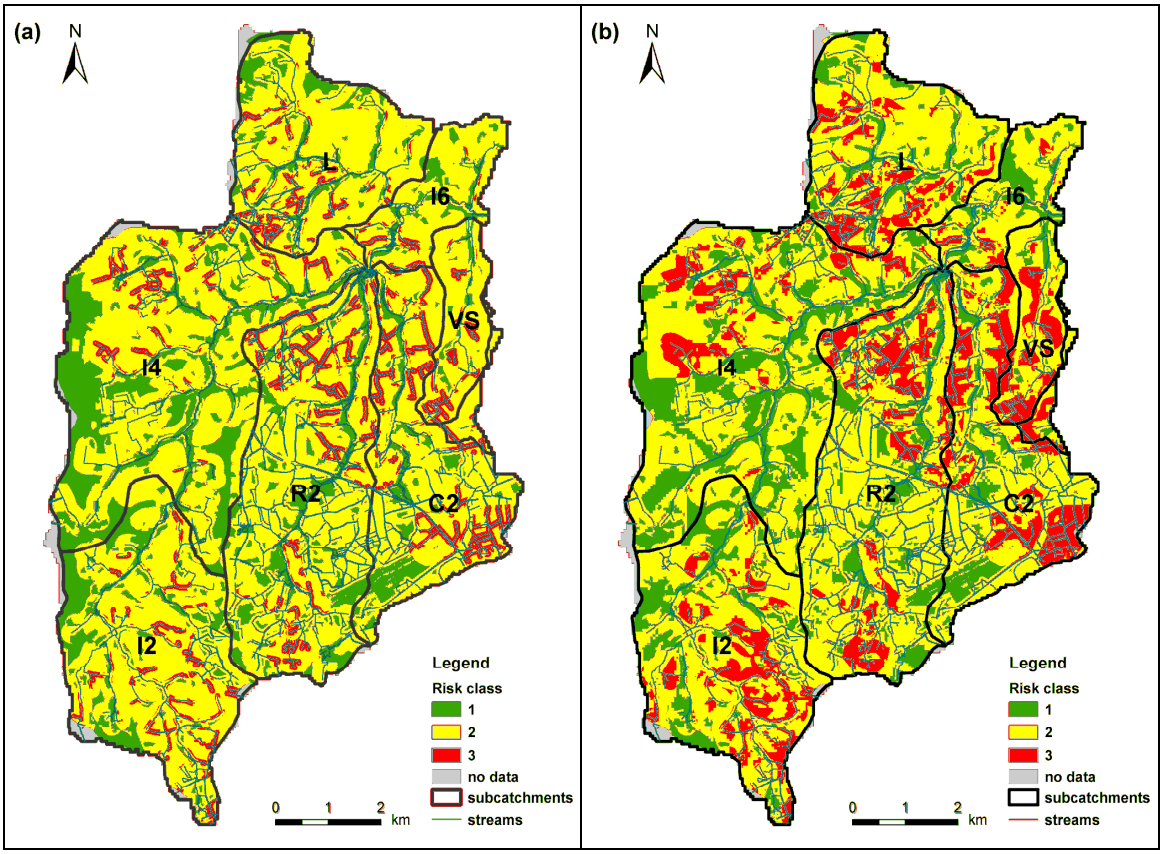

Figure 23. Overlay without parameter *riparian buffer strips* versus full overlay. (a) Overlay without parameter *riparian buffer strips.* (b) Full overlay of five parameters.

Comparison of subcatchment ranking

From the visual comparison of the maps the same conclusions about CSAs would be drawn for the overlays with and without the parameter *riparian buffer strips*. However, a significant change in the ranking is observed for the subcatchment Rodo. Rodo has a particularly dense network of drainage ditches without buffer zones leading to high risk regarding the parameter *riparian buffer strips* (Figure 12), similarly to Camet and Ville

Serho. However, Rodo (together with Ic Centre) is most impacted by low class areas from parameter *soil*. As a result, omitting the parameter *riparian buffer strips* leads to a drop in the ranking of Rodo behind Lantic, Ic Amont and Ic Littoral, which are all predominantly in the high risk area of the parameter *soil*. The inverse reaction can be observed for Rodo when omitting the parameter *soil* (Figure 19).

Table 20. Ranking of subcatchments after overlay without parameter *riparian buffer strips* versus full overlay.

Subcatchment	Without buffer	Rank	Full overlay	Rank
Ville Serho	2.0759	1	2.1375	1
Camet	2.0000	2	2.0871	2
Rodo	1.9407	6*	2.0248	3
Lantic	1.9638	3*	2.0165	4
Ic Amont	1.9452	4*	2.0008	5
Ic Littoral	1.9442	5*	1.9163	6
Ic Centre	1.8351	7	1.8682	7

* rank differs from the one of the full overlay.

NO_3^--N loads versus risk class of parameter riparian buffer strips

Plotting NO_3^--N loads against the parameter *riparian buffer strips* shows a tendency of proportional dependency, similar to the parameter *land use* (Figure 24). However, no significant correlation was found (R^2 = 0.42 (linear model); p-value = 0.12).

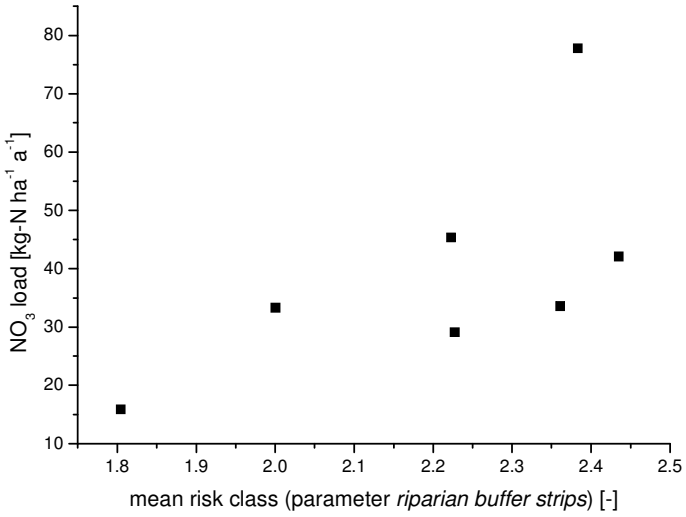

Figure 24. Measured NO_3^--N loads plotted against the mean risk class of the parameter *buffer strips*.

4.2.5 Distance to surface waters

Visual comparison

Similarly to the parameters *land use* and *slope*, omitting the parameter *distance to surface waters* does not influence the spatial distribution of CSAs to a great extent (Figure 25). In contrast to *land use* and *slope* this small effect cannot be solely explained by homogenous distribution of risk classes (Figure 12). However, a dense network of surface waters, in particular drainage ditches, is mainly present in areas, where risk classes are already high. While major changes are not visible, omitting of the parameter leads to broader CSAs including areas in more distance from the stream network.

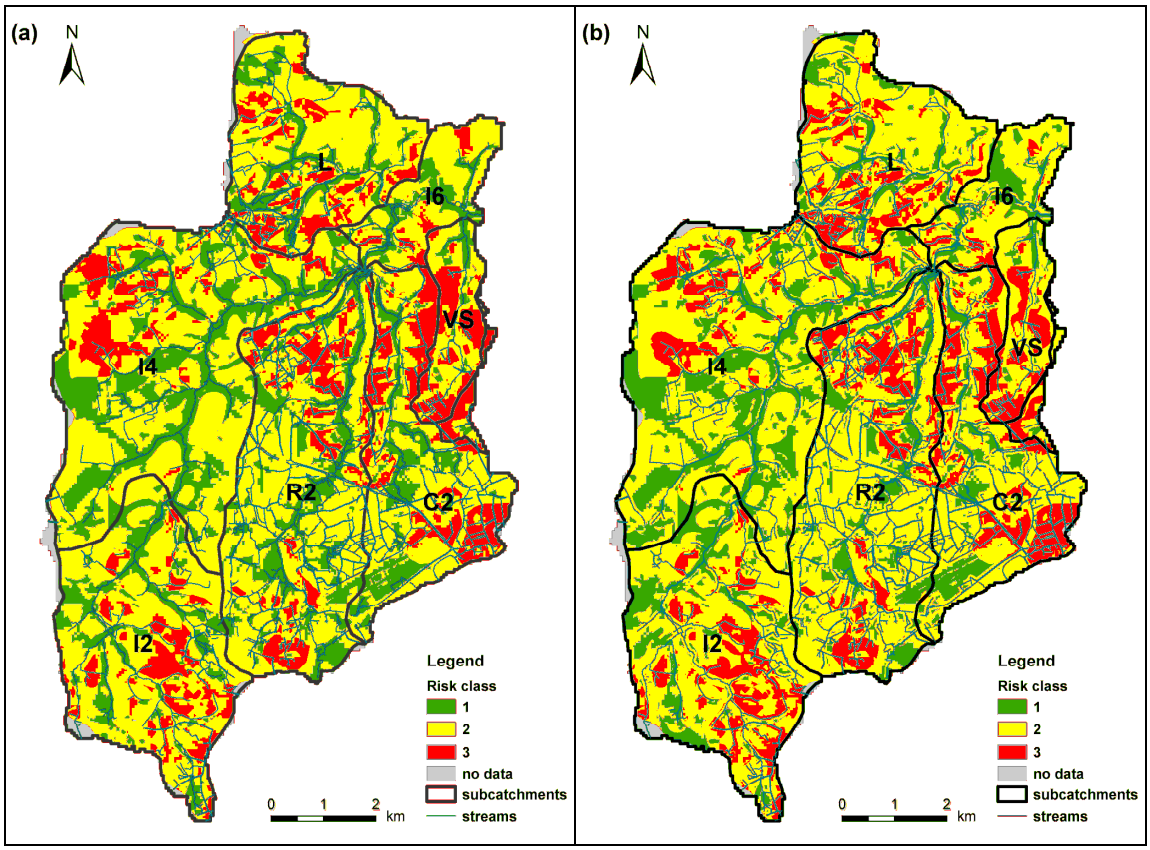

Figure 25. Overlay without parameter *distance to surface waters* versus full overlay. (a) Overlay without parameter *distance to surface waters.* (b) Full overlay of five parameters.

Comparison of subcatchment ranking

The ranking confirms the visual impression that CSAs are very similarly distributed with and without the parameter *distance to surface waters*. However, similarly to the overlay without the parameter *riparian buffer strips*, Rodo results on rank 6 instead of 3 (Table 21). Again, the reason is most likely the distribution of the parameter *soil*, which gains in dominance.

Table 21. Ranking of subcatchments after overlay without parameter *distance to surface waters* versus full overlay.

Subcatchment	Without distance	Rank	Full overlay	Rank
Ville Serho	2.1393	1	2.1375	1
Camet	1.9905	2	2.0871	2
Rodo	1.8990	6*	2.0248	3
Lantic	1.9794	3	2.0165	4
Ic Amont	1.9581	4	2.0008	5
Ic Littoral	1.9081	5	1.9163	6
Ic Centre	1.8311	7	1.8682	7

* rank differs from the one of the full overlay.

NO_3^--N loads versus risk class of parameter distance to surface waters

Considered as a single parameter *distance to surface waters* does not correlate significantly (R^2 = 0.02 (linear model); p-value = 0.78) with the mean risk class (Figure 26). A possible explanation can be that the parameter itself does not have a large influence on the NO_3^--N load in the surface waters. For instance, non-fertilized areas, which do not contribute high NO_3^--N loads, are assigned highest risk class for this parameter if they are located close to a stream. However, the parameter is still sensible, since among the CSAs found in a catchment without the distance parameter, the ones closest to surface waters are likely to contribute more NO_3^- to surface waters.

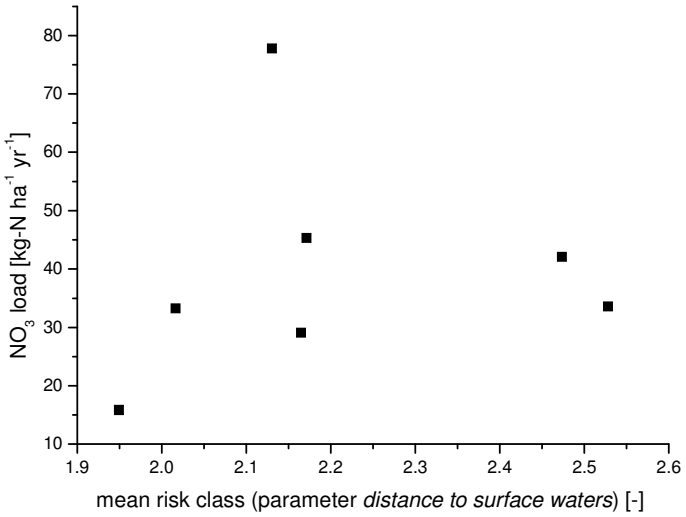

Figure 26. Measured NO_3^--N loads plotted against the mean risk classes of the parameter *distance to surface waters*.

4.3 Comparison and discussion

The GIS overlay seems to be a simple and useful approach for the assessment of CSAs in a catchment. The visual analysis of the results allows a good spatial identification of CSAs on the catchment or subcatchment level. The calculation of average risk class for subcatchments can be used for detailed distinctions.

Validation of results was attempted for the Ic catchment (i) via measured loads in seven sub-catchments and (ii) via simulated loads in 32 subcatchments of the SWAT application. For both validation methods the resulting CSAs in the subcatchments are comparable to the ones in the tested GIS approach despite the differences in size of the detected CSAs (see Chapters 4.1.1 and 4.1.2). The detailed spatial results of the GIS approach are a clear advantage to NO_3^- measurements and SWAT. Therefore, the results of the GIS approach seem to be a good basis for the placement of mitigation zones. However, limits of validation need to be kept in mind. The validation of the approach by measured NO_3^- loads was only possible to a limited extent, because monthly loads had to be used, which do not reflect maximum discharges in the catchment. Furthermore, it is difficult to validate the results with only seven data points. The validation via SWAT is also limited, because reproduction of measured loads was relatively weak (Julich *et al.* 2009) and because of its different aim to predict the actual NO_3^- loads.

The sensitivity analysis for the application to the Ic catchment reveals generally that the GIS overlay is not very sensitive to the single input parameters. For most parameters no more than two of the seven subcatchments change their position in a ranking according to their average risk class. Solely the parameter *soil* has a strong effect on the full overlay, leading to a different ranking of all seven subcatchments and a clear south-north shift of CSAs. But even for this parameter the three subcatchments with the highest mean risk class stay among the top three subcatchments and the four subcatchments with the lowest mean risk class stay among the bottom four subcatchments.

Although sensitivity is lower than expected, it has to be kept in mind that even the change of two subcatchments in the ranking could change the decision on where a mitigation zone is placed. Consequently, single parameters can still have a significant influence on the result. The extent of their influence is strongly dependent on their distribution of the risk classes on the considered spatial scale. For example, in the Ic catchment the parameter *soil* shows high risk in the north and low risk in the south (except Ic Amont, Figure 7). As a result it has a strong impact on risk class distribution on catchment level. However, if only a northern subcatchment is considered *soil* becomes of homogeneous character. In this case, the parameter have a different impact on the CSA identification, because it only decreases or increases the final result.

Because of the importance of single parameters, data quality is a very relevant issue. Regarding the application of the GIS approach to the Ic catchment, especially soil data and drainage ditch information contain some uncertainties. Therefore the strong influence of the parameter *soil* might be especially problematic.

Analysis shows further that most parameters can be linked, which can result in interference. These relations can be quite complex and may determine the occurrence of risk class for several parameters. This can lead to cumulative or antagonistic effects of high and low risk classes. Antagonistic effects could occur for the case of drainage ditches, which are mostly used in impermeable soils, i.e., a higher risk class regarding *distance to surface waters* where the *soil* risk class is low. Another example is agricultural land use that is more probable at low slopes. In turn, cumulative effects are expected for drainage ditches, which are typically more abundant in areas with cropland, i.e., high risk regarding the parameters *land use* and *distance to surface waters.* Similarly, the likelihood for forest or grassland buffers decreases with the increase of cropland area, i.e., high risk regarding *land use* and *riparian buffer strips*.

As mentioned in Chapter 3.4.1, the resulting float values of the overlay were classified into three equidistant risk classes between 1 and 3. The influence of this classification on

the resulting maps becomes apparent using the example of the homogeneous parameter *slope*. Generally, a homogeneous parameter does not contribute to the differentiation between different areas. With the classification it seems that *slope* has a considerable impact on the result, because the visual differences between the overlay with and without slope are distinctive (Figure 21). If the float values of the overlay were shown directly, it would become apparent that all areas receive a lower value when *slope* is included. However, the equidistant classification over the full possible range of 1 to 3 for the overlay results was chosen in order to make overlays comparable even if the results have a different range of values, since, e.g., the maximum value is decreased if a layer with only risk class 1 is included.

Chapter 5
Conclusions

5.1 Results of the study

In this work a universal GIS-based approach for the detection of CSAs of diffuse NO_3^- pollution in rural catchments was tested based on a combination of existing methods. The aim was to provide a ranking of areas regarding their risk of diffuse agricultural NO_3^- pollution instead of predicting NO_3^- loads. The five parameters *land use*, *soil*, *slope*, *riparian buffer strips* and *distance to surface waters* were identified as most relevant for diffuse agricultural NO_3^- pollution. Each of the parameters was classified into the following three risk classes: low (1), moderate (2) and high (3) risk of NO_3^- pollution (Chapter 3.3). For a test application of the approach the five parameters were combined with equal weight in an overlay in order to find areas with highest risk (Chapter 3.4).
The Ic catchment in Brittany, France, served as a study site to test the applicability of the GIS approach. For validation, the GIS overlay was compared (i) with measured NO_3^- loads in seven subcatchments of the Ic (Chapter 4.1.1) and (ii) with previous results of the hydrological model SWAT (Chapter 4.1.2). Regarding (i), the validation revealed a general relation between the mean risk class in a subcatchment and the corresponding measured NO_3^- load. However, because of the small number of only seven data points a reliable statistical analysis was not possible. Regarding (ii), the plotting of predicted loads by SWAT versus the mean risk class for the 32 SWAT subcatchments showed poorer agreement. This might be due to the substantial differences in the approaches and in the used data sets. Nevertheless, in a visual comparison the areas with most predicted CSAs by the GIS approach coincide well with the predicted hotspots by SWAT, except for some areas in the west of the catchment. Compared to the result of the SWAT analysis, CSAs predicted by the GIS overlay are more fragmented, i.e., they include more spatially detailed information.
The GIS overlay was further analyzed regarding its sensitivity to each of the five parameters (Chapter 4.2). This analysis showed that the overlay is not very sensitive to single parameters, i.e., no major change in results occurs if one parameter is omitted. In the case of the Ic, higher sensitivity was only found for the parameter *soil*. This is due to the clear zoning of the catchment into a high risk and a low risk area. But even if omitting this parameter the three subcatchments with the highest mean risk classes stay among the top three subcatchments and the four subcatchments with the lowest mean risk classes stay among the bottom four subcatchments. Given the test application for the Ic

catchment, it is concluded that the tested GIS overlay is relatively robust, even if information for one parameter is missing in a given catchment.
The example of the parameter *soil* shows that the sensitivity of the method to a parameter depends very much on the spatial distribution of risk classes. It was found that parameters have the highest impact on overlay results if they show a clear zoning (e.g., 50 % of subcatchments are risk class 1 and 50 % of subcatchments are risk class 3) rather than homogenous fragmentation. Particularly for such 'high-impact' parameters, the issue of data quality emerges. In the Ic catchment this is the case for the parameter *soil*, which has a comparably high impact on results but is based on data of uncertain quality as explained in Chapter 3.3.2. However, as the challenge of data quality will be present in many rural catchments, the Ic catchment can be seen as quite representative.
A further issue is the identifiability of parameters. Even though it was attempted to use parameters which are independent from each other, complex dependencies cannot be avoided in all cases. Such dependencies can lead to cumulative or antagonistic effects regarding the overall risk classes (Chapter 4.3). While possible dependencies make correlation with actual loads difficult, they may also support robustness of the approach.

In summary, the tested GIS approach is relatively simple to use. The clear distinction of parameters in separate risk maps makes it very flexible, providing a good applicability to catchments with different data availabilities, since parameters can be removed or updated without influencing the other parameters. The results of a simple overlay of five parameters have further shown low sensitivity to the omission of single parameters.

5.2 Recommendation for development of a universal GIS method

A GIS overlay of separate risk maps of nitrate pollution seems to be a promising approach for CSA identification, given its relatively simple application, its high flexibility to varying data availability and its high transparency of how final results were achieved. Moreover, a first test with five equally weighted parameters showed reasonable correlation with other CSA identification methods (load estimations from measurements, SWAT simulation). However, several open points need to be assessed to move towards the development of a future GIS method, universally applicable to catchments, which are subject to diffuse agricultural pollution. Open points are discussed in the following subsections.

5.2.1 Number of classes

It should be mentioned that overlay will only rarely result in areas with risk class 3. As a result, highest risk in a catchment more generally corresponds with the highest value of the overlay results. In order to get a better distinction of the areas with different risk it would be possible to display the results in more classes than just three.

Further distinction could be reached by using more than three classes for single parameters (e.g., slope), if data availability and parameter allow. In further method development a flexible number of classes could be imagined for each parameter. The user could then choose to increase the number of classes for parameters with good data availability. Higher or lower number of classes for single parameters could easily be normalized to a common scale (e.g., to a 1-3 scale in the above study) before the overlay to avoid weighting effects.

While increasing the number of classes for parameters with good data availability may make sense in many cases, one has to keep in mind that a simple GIS approach is qualitative and there is a risk to feign precision.

5.2.2 Weighting of parameters

Most available methods apply some sort of weighting of parameters; often without a clear basis. In the present study, definition of weights was attempted by multiple linear regressions of measured loads versus the five parameters defined above. The analysis did not provide a sensible model, mainly because risk classes cannot be compared directly to measured loads. Moreover, such a weighting would be catchment-specific.

Nevertheless, catchment-specific weighting could be applied, either via local expert knowledge or general aspects. When applying weighting it is important to make its effect transparent to avoid (i) incomprehensible results and (ii) to loose one of the main advantages of the GIS overlay.

One systemic, transferable weighting approach was used by Vernoux et al. (2007) for the assessment of areas which pose a risk for groundwater contamination from diffuse pollution. They grouped parameters into a “vulnerability” and a “pressure” map, which were weighted equally in a final overlay. In the case of the tested approach “pressure” would be represented by the *land use* map, whereas “vulnerability” would comprise transport (*soil*, *slope*) and retention (*distance to surface water*, *buffer strips*) parameters. Then, a direct overlay of “vulnerability” and “pressure” maps would correspond to a weight of 4 for the parameter *land use*.

5.2.3 Transport parameters

Transport of nitrogen is rendered more complex by the fact that it can enter surface waters via (i) subsurface/groundwater pathway, (ii) surface runoff in dissolved or particulate form and (iii) tile drainage. For the large and diverse German Elbe River (catchment ~100000 km^2) diffuse agricultural loads of nitrogen are dominated by groundwater pathway (~66 %), followed by tile drainage (~26 %) and surface runoff (~5 %) (Arbeitsgemeinschaft für die Reinhaltung der Elbe 2001). The dominance of the groundwater pathway was confirmed also for the peri-alpine rivers of the German Danube catchment (~81 % of agricultural nitrogen inputs; Bayerisches Staatsministerium für Umwelt und Gesundheit 2009a), the German Rhine catchment (~81 %; Bayerisches Staatsministerium für Umwelt und Gesundheit 2009b) and the Swiss Rhine catchment (~81 %; Prasuhn 2003). Both tile drainage, as well as surface runoff vary between 4 % and 13 % contribution in those three catchments.

Given these relations, most approaches consider only the groundwater passage for nitrate risk areas. If the three major agricultural pathways are considered this leads to the following difficulties:

- When combining groundwater and surface runoff parameters in an overlay the two parameters can cancel each other out. For instance, if soil is well permeable nitrate leaching risk is high but risk for surface runoff is low; as a result overlay would result in average risk for all surfaces. One option in a further development of the method would be to supply two vulnerability maps, one for groundwater pathway and one for surface runoff, and include them depending on local conditions.
- While leaching via interflow and groundwater is the dominant nitrogen pathway to surface water in most catchments, the point of connection of the groundwater below a specific field to a surface water body is typically unknown. However, the longer the subsurface pathway the higher the probability of denitrifying processes on the way. The problem is less expressed for interflow which can be assumed to follow roughly the topography.
- One particular issue is the third important pathway via tile drainage. Although the load via tile drainage is clearly lower than groundwater pathway in the above examples of large catchments, it can (a) dominate locally and (b) lead to concentration peaks during storm events (DWA 2008). In particular, agriculturally-

used, impermeable soils are likely to be drained by drainage pipes, but receive a low risk class for the parameter *soil* in the tested GIS approach. However, locations of tile drains are unknown in most catchments. The issue could be tackled by assigning cropland with impermeable soils a high risk class (e.g., +1), either in the parameter *soil* directly or in the parameter *distance to surface waters* (since drainage pipes are basically an artificial extension of the river network).

5.2.4 Testing of a developed GIS method

Before applying a newly developed GIS method to catchments for CSA identification, it should preferably be tested on several catchments with readily available data or at least different data gaps. The applied validation via load measurements and other approaches (in this case SWAT) is suggested to be applied similarly. As a result, good estimates of NO_3^- load should be available in test catchments. Moreover a sensitivity analysis, analogous to the one performed in chapter 4.2 of this study, is recommended, since the sensitivity of the developed method to data gaps is crucial.

5.2.5 Application of GIS-based methods

In practical use, GIS-based methods could be applied to catchments characterized by agricultural NO_3^- problems. Depending on the size of the analyzed catchment and the size of the resulting risk areas, the results could (i) indicate larger risk areas to focus mitigation measures on, (ii) locate directly potentially suitable sites for the placement of mitigation zones or (iii) compare possible mitigation areas regarding the risk for NO_3^- pollution of their watersheds.

However, GIS-based CSA identification can only be a first step and reality check in the field is required. For the detailed planning of measures, local information (soil type, topography, cooperation of land-owner, etc.) needs to be collected and cannot be replaced by a GIS-based approach.

References

Aber, J. D., K. J. Nadelhoffer, P. Steudler, and J. M. Melillo. 1989. Nitrogen Saturation in Northern Forest Ecosystems. ***BioScience*** 39**:** 378-386.

Ad-hoc-Arbeitsgruppe Boden. 2005. Bodenkundliche Kartieranleitung, 5th edition ed. Bundesanstalt für Geowissenschaften und Rohstoffe.

Arbeitsgemeinschaft für die Reinhaltung der Elbe. 2001. Analyse der Nährstoffkonzentrationen, -frachten und -einträge im Elbeeinzugsgebiet, p. 90. *In* H. Reincke [ed.].

Auth, S., S. Forstner, P.-M. Rintelen, M. Halama, and K. Auerswald. 2005. Nährstoffbelastungen der Gewässer durch die Landwirtschaft - Methoden zur Abschätzung, Möglichkeiten zur Reduzierung Bayerische Landesanstalt für Landwirtschaft.

Bae, M. S., and S. R. Ha. 2005. GIS-based influence analysis of geomorphological properties on pollutant wash-off in agricultural area. ***Water Science and Technology*** 51**:** 301-307.

Basnyat, P., L. D. Teeter, B. G. Lockaby, and K. M. Flynn. 2000. The use of remote sensing and GIS in watershed level analyses of non-point source pollution problems. ***Forest Ecology and Management*** 128**:** 65-73.

Baß, S., R. Fahrner, T. Kowalke, H. Bogenschütz, D. Kaltenmeier, and J. Mair. 2005. WRRL; Bericht Teilbearbeitungsgebiet "Wutach". Regierungspräsidium Freiburg.

Bayerisches Staatsministerium für Umwelt und Gesundheit. 2009a. Bewirtschaftungsplan für den bayerischen Anteil der Flussgebietseinheit Donau. Die Europäische Wasserrahmenrichtlinie und ihre Umsetzung in Bayern. Bayerisches Landesamt für Umwelt.

Bayerisches Staatsministerium für Umwelt und Gesundheit. 2009b. Bewirtschaftungsplan für den bayerischen Anteil der Flussgebietseinheit Rhein. Die Europäische Wasserrahmenrichtlinie und ihre Umsetzung in Bayern. Bayerisches Landesamt für Umwelt.

BDPA SCET AGRI. 1987. Carte des sols au 1/100000. Departement des Cotes du Nord - Direction Departamentale de L'agriculture et de la Foret.

BDPA SCET AGRI. 1988. Carte des sols au 1/100000 - Notice. Departement des Cotes du Nord - Direction Departementale de L'agriculture et de la Foret.

Beaulac, M. N., and K. H. Reckhow. 1982. Examination of land use - nutrient export relationships. ***Water Resources Bulletin*** 18**:** 1013-1024.

Brunet, R.-C., K. B. Astin, S. Dartiguelongue, and P. Brunet. 2008. The mineralisation of organic nitrogen: Relationship with variations in the water-table within a floodplain of the River Adour in southwest France. ***Water Resources Management*** 22**:** 277-289.

Bugey, A. 2009. Methods for the assessment of diffuse nutrient pollution in rural catchments. Project report Aquisafe 1. Kompetenzzentrum Wasser Berlin gGmbH.

Central Intelligence Agency. 2009. The World Factbook. France. Central Intelligence Agency. https://www.cia.gov/library/publications/the-world-factbook/geos/fr.html

Chambre d'Agriculture de l'Aisne. 2007. Identifiez votre sol. Conseil Général L'Aisne; Chambre d'Agriculture de l'Aisne; INRA.

Crétaz, A., and P. K. Barten. 2007. Land Use Effects on Streamflow and Water Quality in the Northeastern United States. CRC Press.

Di, H. J., and K. C. Cameron. 2002. Nitrate leaching in temperate agroecosystems: Sources, factors and mitigating strategies. ***Nutrient Cycling in Agroecosystems*** 64**:** 237-256.

Dise, N. B., and R. F. Wright. 1995. Nitrogen leaching from European forests in relation to nitrogen deposition. ***Forest Ecology and Management*** 71**:** 153-161.

DWA. 2008. Dränung: Nährstoffausträge, Flächenerfassung und Management, p. 114. DWA Themen. Deutsche Vereinigung für Wasserwirtschaft, Abwasser und Abfall e.V.

Environmental Systems Research Institute. 2005a. Creating a depressionless DEM. Environmental Systems Research Institute (ESRI). http://webhelp.esri.com/arcgisdesktop/9.1/index.cfm?TopicName=Creating%20a%20depressionless%20DEM

Environmental Systems Research Institute. 2005b. ArcGIS.

European Environment Agency. 2000. Corine land cover - data downlaod for year 2000. European Environment Agency. http://www.eea.europa.eu/themes/landuse/clc-download

Foster, I. D. L., B. W. Ilbery, and M. A. Hinton. 1989. Agriculture and water quality: a preliminary examination of the Jersey nitrate problem. ***Applied Geography*** 9**:** 95-113.

Franko, U., T. Schmidt, and M. Volk. 2001. Modellierung des Einflusses von Landnutzungsänderungen auf die Nitrat-Konzentration im Sickerwasser, p. 165 - 186. *In* H. Horsch, I. Ring and F. Herzog [eds.], Nachhaltige Wasserbewirtschaftung und Landnutzung. Methoden und Instrumente der Entscheidungsfindung und -umsetzung. Metropolis-Verlag.

Gilliam, J. W., D. L. Osmond, and R. O. Evans. 1997. Selected Agricultural Best Management Practices to Control Nitrogen in the Neuse River Basin. North Carolina Agricultural Research Service Technical Bulletin 311. North Carolina State University.

Heinzmann, B. 1993. Beschaffenheit und weitergehende Aufbereitung von städtischen Regenabflüssen. VDI-Verlag.

Hickey, R. 2000. Slope Angle and Slope Length Solutions for GIS. ***Cartography*** 29**:** 1-8.

INRA. 2008. Etude sur les bassins versants en contentieux «nitrates eaux brutes», p. 233. INRA.

Jordan, C. 1994. Modelling of nitrate leaching on a regional scale using a GIS. ***Journal of Environmental Management*** 42**:** 279-298.

Jordan, F., C. Müller, and P. Holleis. 2004. Oberflächenabfluss, Boden- und Nährstoffaustrag. http://www.lfl.bayern.de/iab/bodenschutz/08131/

Jordan, T. E., D. L. Correll, and D. E. Weller. 1993. Nutrient interception by a riparian forest receiving inputs from adjacent cropland. ***Journal of Environmental Quality*** 22**:** 467-473.

Julich, S., L. Breuer, and H.-G. Frede. 2009. Hydrological and nitrate modelling for the River Ic in Brittany (France) - Simulation results and pre-liminary scenario analysis. Project Report Aquisafe 1 Extension. Kompetenzzentrum Wasser Berlin gGmbH.

Julich, S., L. Breuer, and H.-G. Frede. in press. Hydrological and nitrate modelling for the River Ic in Brittany (France) - Simulation results and pre-liminary scenario analysis. Project Report Aquisafe 1 Extension. Kompetenzzentrum Wasser Berlin gGmbH.

Karr, J. R., and I. J. Schlosser. 1978. Water resources and the land-water interface. Water resources in agricultural watersheds can be improved by effective multidisciplinary planning. ***Science*** 201**:** 229-234.

Kaste, Ã., A. Henriksen, and A. Hindar. 1997. Retention of atmospherically-derived nitrogen in subcatchments of the Bjerkreim River in southwestern Norway. ***Ambio*** 26**:** 296-303.

King, R. S., M. E. Baker, D. F. Whigham, D. E. Weller, T. E. Jordan, P. F. Kazyak, and M. K. Hurd. 2005. Spatial considerations for linking watershed land cover to ecological indicators in streams. ***Ecological Applications*** 15**:** 137-153.

Kuderna, M., M. Pollak, and E. Murer. 2000. Überprüfung von drei in Österreich üblichen Modellansätzen zur Ermittlung der Nitrataustragsgefährdung. Amt der

oberösterreichischen Landesregierung; Bundesministerium für Land- und Forstwirtschaft.

Ley, T. W., R. G. Stevens, R. R. Topielec, and W. H. Neibling. 1994. Soil Water Monitoring and Management. Pacific Northwest states—Washington, Oregon, and Idaho (PNW Program). http://cru.cahe.wsu.edu/CEPublications/pnw0475/pnw0475.html#anchor1601641

Magdoff, F., L. Lanyon, and B. Liebhardt. 1997. Nutrient cycling, transformations, and flows: Implications for a more sustainable agriculture. ***Advances in Agronomy*** 60**:** 1-73.

Maillard, P., and N. A. Pinheiro Santos. 2008. A spatial-statistical approach for modeling the effect of non-point source pollution on different water quality parameters in the Velhas river watershed - Brazil. ***Journal of Environmental Management*** 86**:** 158-170.

Mattikalli, N. M., and K. S. Richards. 1996. Estimation of surface water quality changes in response to land use change: Application of the export coefficient model using remote sensing and geographical information system. ***Journal of Environmental Management*** 48**:** 263-282.

Mayer, P. M., S. K. Reynolds Jr., and T. J. Canfield. 2005. Riparian buffer width, vegetative cover, and nitrogen removal effectiveness: A review of current science and regulations, p. 27. U.S. Environmental Protection Agency.

McCulloch, J. S. G., and M. Robinson. 1993. History of forest hydrology. ***Journal of Hydrology*** 150**:** 189-216.

Munafo, M., G. Cecchi, F. Baiocco, and L. Mancini. 2005. River pollution from non-point sources: A new simplified method of assessment. ***Journal of Environmental Management*** 77**:** 93-98.

MUNLV. 2005. Umsetzung der Europäischen Wasserrahmenrichtlinie in Nordrhein-Westfalen. Teil 1: Leitfaden zur Bestandsaufnahme, p. 316. Ministerium für Umwelt und Naturschutz, Landwirtschaft und Verbraucherschutz des Landes Nordrhein-Westfalen (MUNLV).

Nearing, M. A. 1997. A single, continuous function for slope steepness influence on soil loss. ***Soil Science Society of America Journal*** 61**:** 917-919.

Nieder, R. 2009. Stickstoff-Überschuss in der Landwirtschaft Deutschlands: Folgen für Böden, Gewässer und angrenzende Ökosysteme. Aktiver Klimaschutz und Anpassung an den Klimawandel – Beiträge der Agrar- und Forstwirtschaft. Fachtagung 15. - 16. Juni. vTI.

Peterjohn, W. T., and D. L. Correll. 1984. Nutrient dynamics in an agricultural watershed: observations on the role of riparian forest. ***Ecology*** 65**:** 1466-1475.

Prasuhn, V. 2003. Entwicklung der Phosphor- und Stickstoffverluste aus diffusen Quellen in die Gewässer im Rheineinzugsgebiet der Schweiz unterhalb der Seen (1985, 1996, 2001), p. 21. Eidgenössische Forschungsanstalt für Agrarökologie und Landbau, Zürich-Reckenholz.

Renger, M. 2002. Sicker- und Fließzeiten von Nitrat aus dem Wurzelraum ins Grundwasser. Arbeitsberichte der TA-Akademie. Akademie für Technikfolgenabschätzung in Baden-Württemberg.

Scheffer, F. 1989. Lehrbuch der Bodenkunde [Scheffer; Schachtschabel], 12th edition ed. Enke.

Schlecker, E. 2003. Leitfaden zum Aufbau eines Landschafts-Informationssystems zur Erfassung diffuser Nährstoffeinträge aus der Landwirtschaft am Beispiel der Seefelder Aach, p. I-82. Albert-Ludwigs-Universität Freiburg, Institut für Landespflege.

Schulze, E. D., W. De Vries, M. Hauhs, K. Rosen, L. Rasmussen, C. O. Tamm, and J. Nilsson. 1989. Critical loads for nitrogen deposition on forest ecosystems. ***Water, Air, and Soil Pollution*** 48**:** 451-456.

Sivertun, A., L. E. Reinelt, and R. Castensson. 1988. A GIS method to aid in non-point source critical area analysis. ***International Journal of Geographical Information Systems*** 2**:** 365-378.

Sivertun, A., and L. Prange. 2003. Non-point source critical area analysis in the Gisselo watershed using GIS. ***Environmental Modelling and Software*** 18**:** 887-898.

Skop, E., and P. B. Sørensen. 1998. GIS-based modelling of solute fluxes at the catchment scale: A case study of the agricultural contribution to the riverine nitrogen loading in the Vejle Fjord catchment, Denmark. ***Ecological Modelling*** 106**:** 291-310.

SMCG/GOËL'EAUX. 2007. Etude Prealable a la Mise en place d'un Contract Restauration Entretien Rivieres & zones humides. Le programme d'amélioration de la qualité des eaux de l'Ic et du Leff Bassin versant de l'Ic, côtiers de Plérin et Pordic. Volet Général., p. 72. SMCG/GOËL'EAUX.

Strube, T. 2009. Selection of a watershed model used to predict the effects of management decisions on water quality based on multi-criteria comparison. Project report Aquisafe 1. Kompetenzzentrum Wasser Berlin gGmbH.

Trepel, M., and L. Palmeri. 2002. Quantifying nitrogen retention in surface flow wetlands for environmental planning at the landscape-scale. ***Ecological Engineering*** 19**:** 127-140.

Umweltbundesamt. 2008a. Critical Loads für Eutrophierung. Umweltbundesamt. http://www.umweltbundesamt-umwelt-deutschland.de/umweltdaten/public/theme.do?nodeIdent=3598

Umweltbundesamt. 2008b. Daten zur Umwelt. Waldzustand in Deutschland. http://www.umweltbundesamt-umwelt-deutschland.de/umweltdaten/public/theme.do?nodeIdent=3190

Umweltbundesamt. 2008c. Daten zur Umwelt. Indikator: Überschreitung der Critical Loads für Stickstoff (Eutrophierung) Umweltbundesamt. http://www.umweltbundesamt-umwelt-deutschland.de/umweltdaten/public/theme.do?nodeIdent=2870

USDA. n. d. Soil Texture Calculator. United States Department of Agriculture. Natural Resources Conservation Service. http://soils.usda.gov/technical/aids/investigations/texture/

Vernoux, J. F., A. Wuilleumier, J.-J. Seguin, and N. Doerfliger. 2007. Méthodologie de délimination des bassins d'alimentation des captages et de leur vulnérabilité vis-à-vis des pollutions diffuses. Rapport intermédiaire: synthèse bibliographique et analyse des études réalisées sur le bassin Seine-Normandie, p. 128. BRGM.

Weigel, A., R. Russow, and M. Körschens. 2000. Quantification of airborne N-input in long-term field experiments and its validation through measurements using 15N isotope dilution. ***Journal of Plant Nutrition and Soil Science*** 163**:** 261-265.

Welsch, D. J. 1991. Riparian Forest Buffers: Function And Design For Protection And Enhancement Of Water Resources. USDA Forest Service, Northeastern Area.

Wendland, F., H. Albert, M. Bach, and R. Schmidt [eds.]. 1993. Atlas zum Nitratstrom in der Bundesrepublik Deutschland. Springer.

Wenger, S. 1999. A review of the scientific literature on riparian buffer width, extent and vegetation. University of Georgia, Institute of Ecology, Office of Public Service & Outreach.

Wishmeier, W. H., and D. D. Smith. 1965. Predicting Rainfall Erosion Losses from Cropland East of Rocky Mountains. U.S. Department of Agriculture.

Appendix

A – Data preparation

A 1. Creation of the depressionless DEM for the Ic catchment

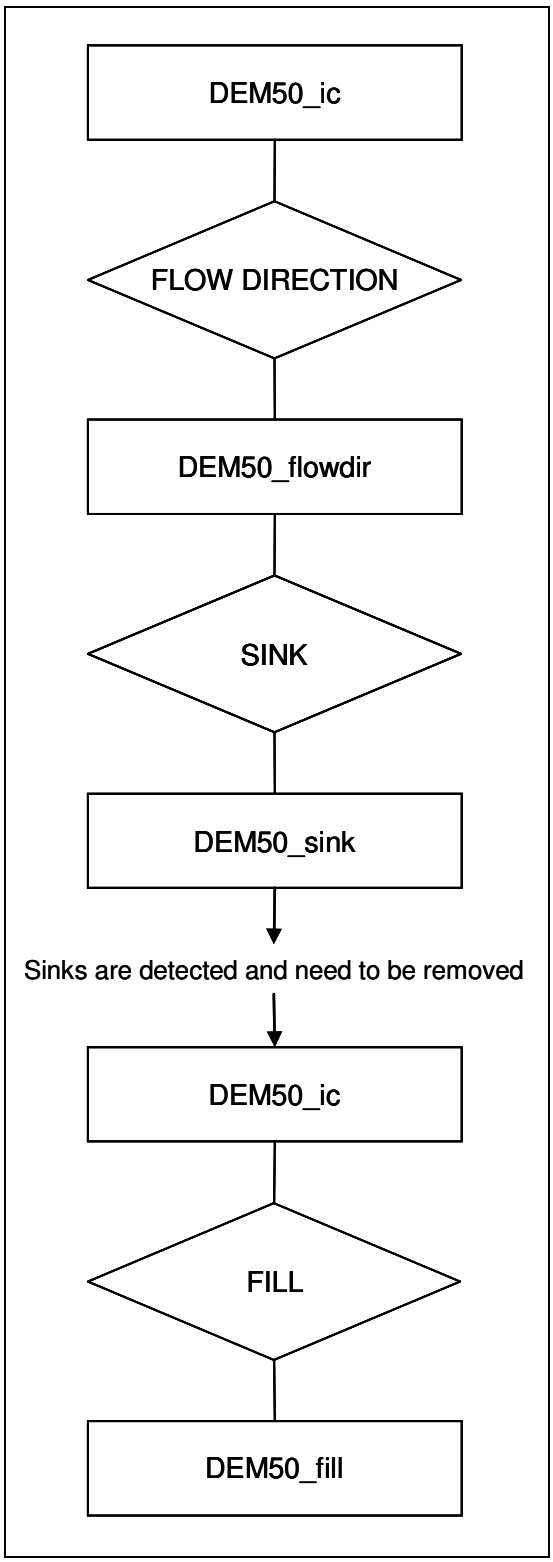

B – Additional information regarding single parameters

B 1. Creation of the risk map of the parameter *land use* for the Ic catchment.

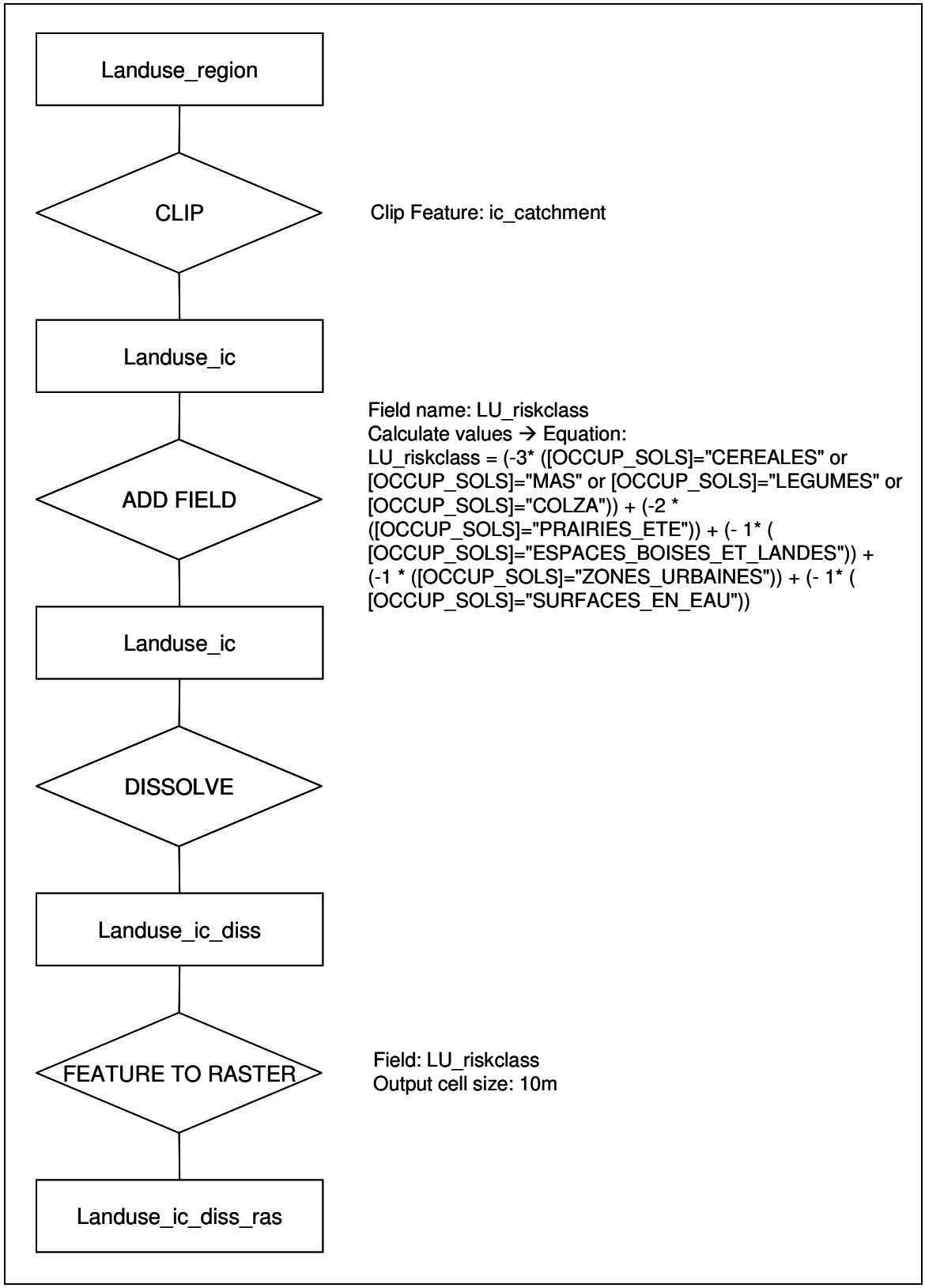

B 2. Additional information on the 10 soil classes defined for the lc catchment.

Soil class	Soil texture (French)	Clay [%]	Silt [%]	Sand [%]	AWC [mm/cm][1)]	min. RZ_{eff} [cm][2)]	max. RZ_{eff} [cm][2)]	min. RZAWC [mm]	max. RZAWC [mm]	Risk class	Corresponding German soil textures
SL	Sable limoneux	0-12	7-45	55-80	1.00	80	90	80	90	3	Su2, Su3, Su4, Sl2, Sl3, (Ss, Sl3)
SL60	Sable limoneux	0-12	7-45	55-80	1.00	> 0	60	> 0	60	3	Su2, Su3, Sl2, Sl3, (Ss, Sl3)
LMS	Limon moyen sableux	7-17	47-77	15-35	1.65	120	200	198	330	1	Uls, (Ut2, Ut3, Slu)
LMS60	Limon moyen sableux	7-17	47-77	15-35	1.65	> 0	60	> 0	99	3*	Uls, (Ut2, Ut3, Slu)
LS	Limon sableux	7-17	37-57	35-55	1.55	120	200	186	310	1	Slu, Uls (Sl3, Sl4)
LS60	Limon sableux	7-17	37-57	35-55	1.55	> 0	60	> 0	93	3*	Slu, Uls (Sl3, Sl4)
LSA	Limon sablo-argileux	17-30	20-47	35-55	1.65	120	200	198	330	1	Ls3, Ls4, Lts, (Lt2, Ls2)
LSA60	Limon sablo-argileux	17-30	20-47	35-55	1.65	> 0	60	> 0	99	3*	Ls3, Ls4, Lts, (Lt2, Ls2)
LAS	Limon argilo sableuse	17-30	35-67	15-35	1.80	100	200	180	360	1	Lu, Ls2, Ls3, (Ut4, Lt2, Tu4)
LAS60	Limon argilo sableuse	17-30	35-67	15-35	1.80	> 0	60	> 0	108	3*	Lu, Ls2, Ls3, (Ut4, Lt2, Tu4)

[1)] Data provided by SMEGA; [2)] Chambre d'Agriculture de l'Aisne 2007; * = the value could also be 2, because the range of possible RZAWC values overlaps both with risk class 2 and 3. Risk class 3 was chosen because the overlapping with this class is predominant.

B 3. Creation of the risk map of the parameter *soil* for the Ic catchment.

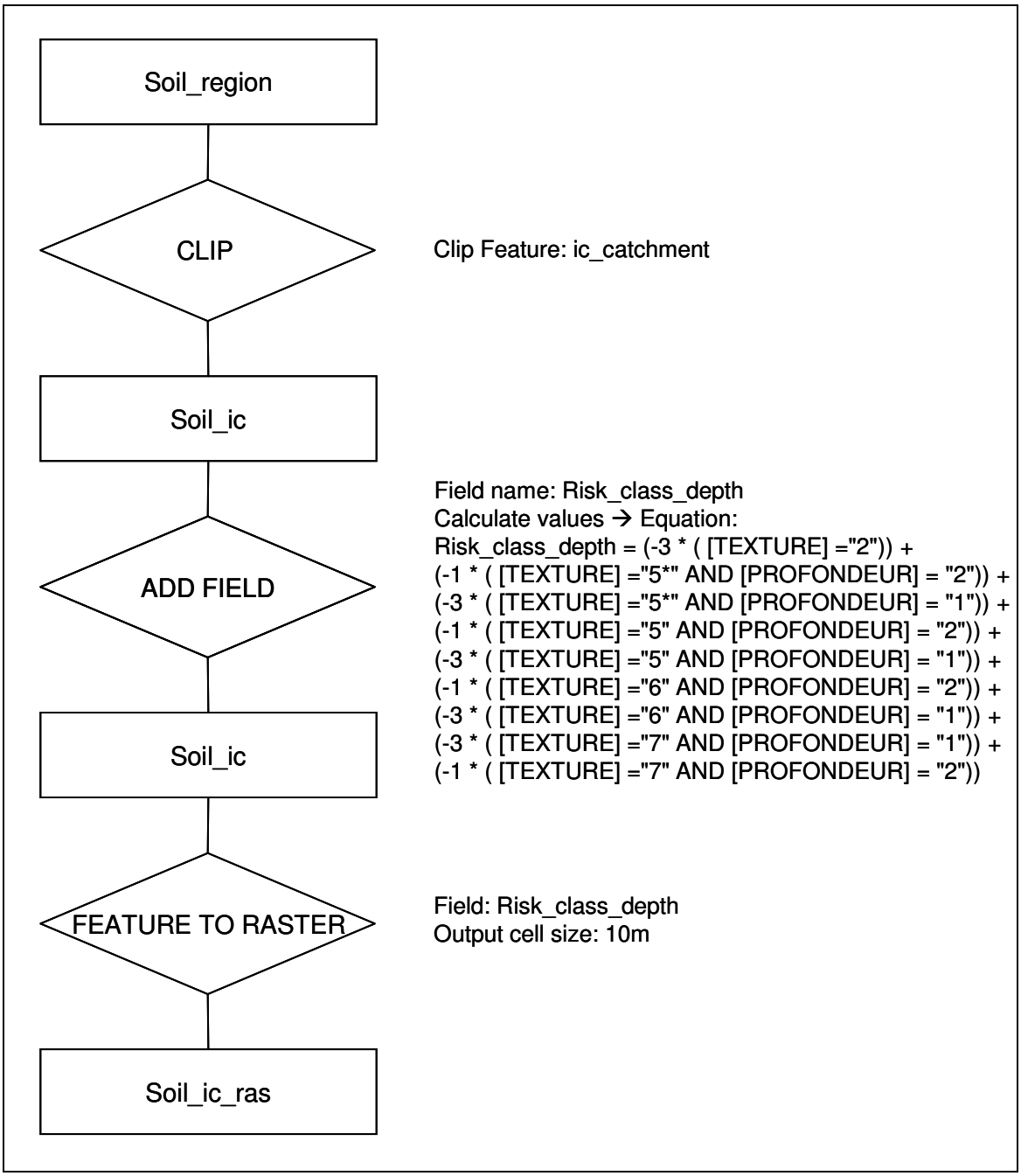

B 4. Creation of the risk map of the parameter *slope* for the Ic catchment.

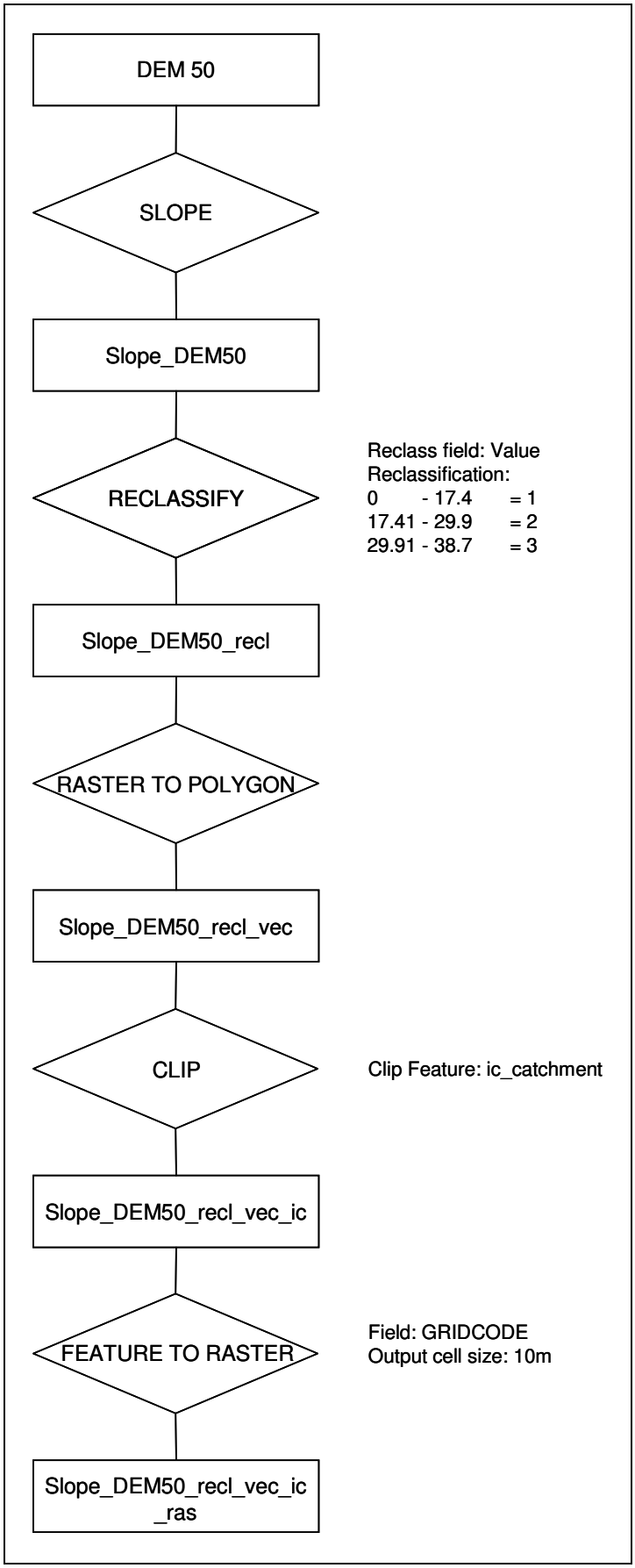

B 5. Creation of the risk map of the parameter *riparian buffer strips* for the Ic catchment.

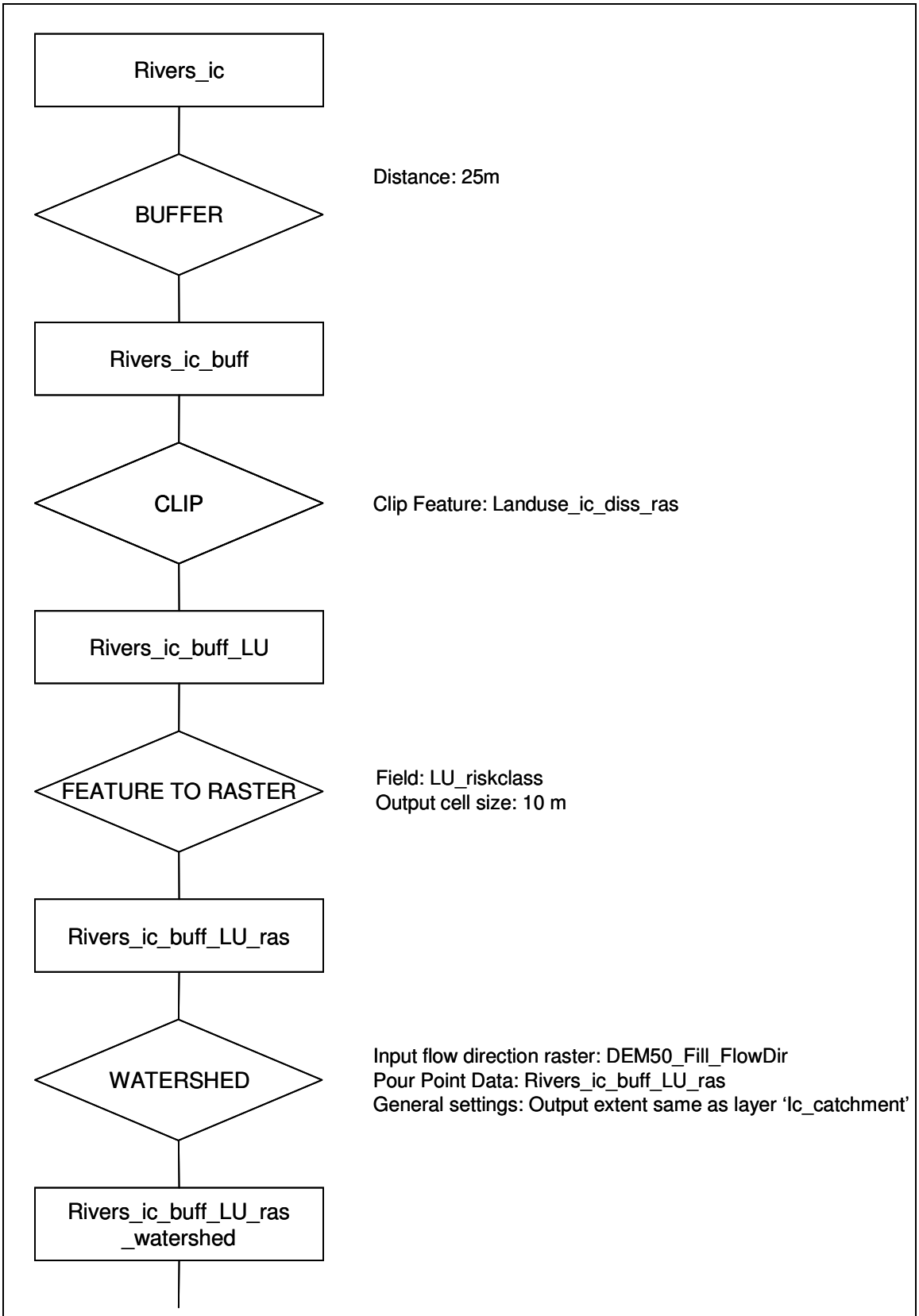

continued on the next page

continued from page 86

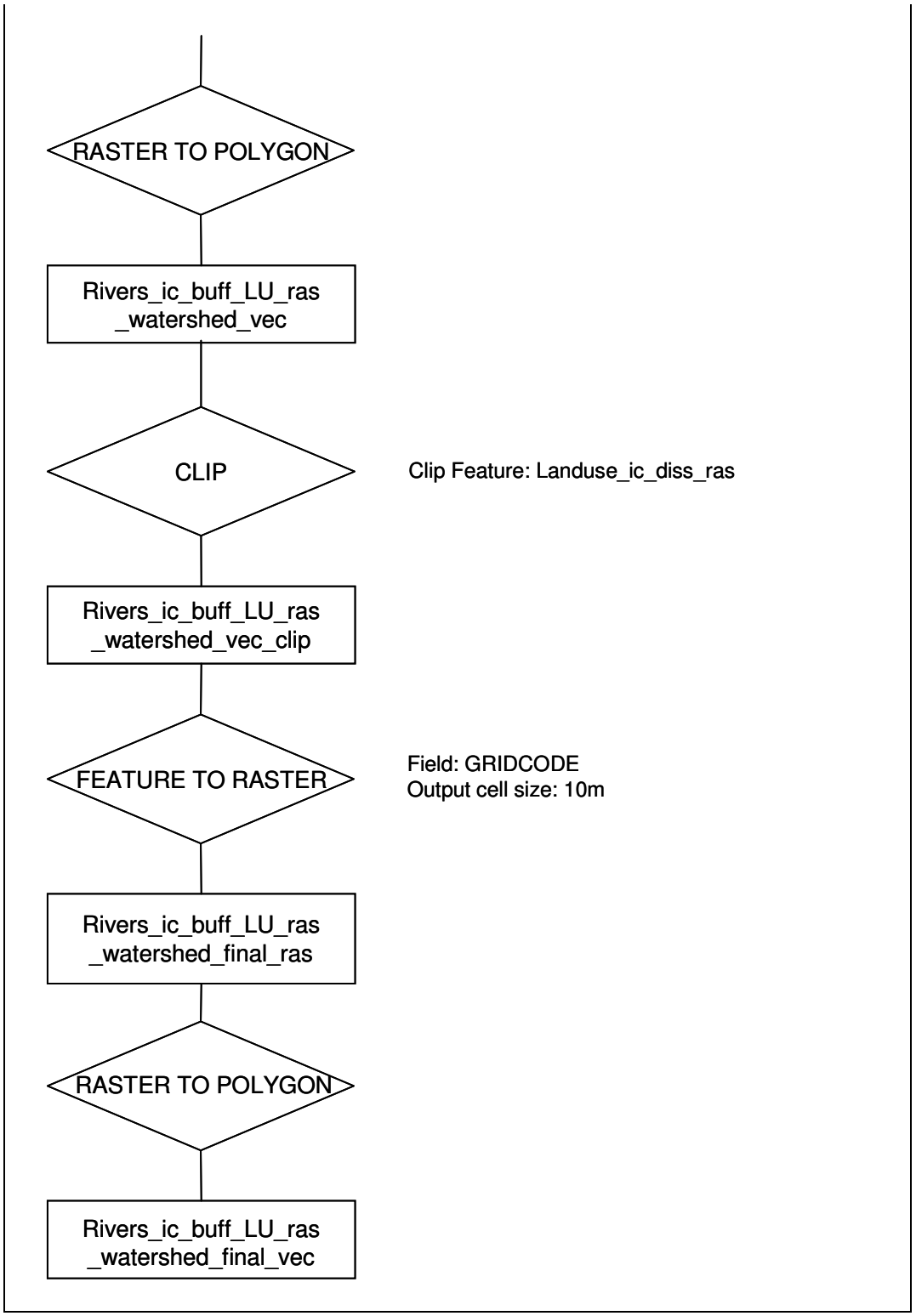

B 6. Creation of the risk map of the parameter *distance to surface waters* for the Ic catchment.

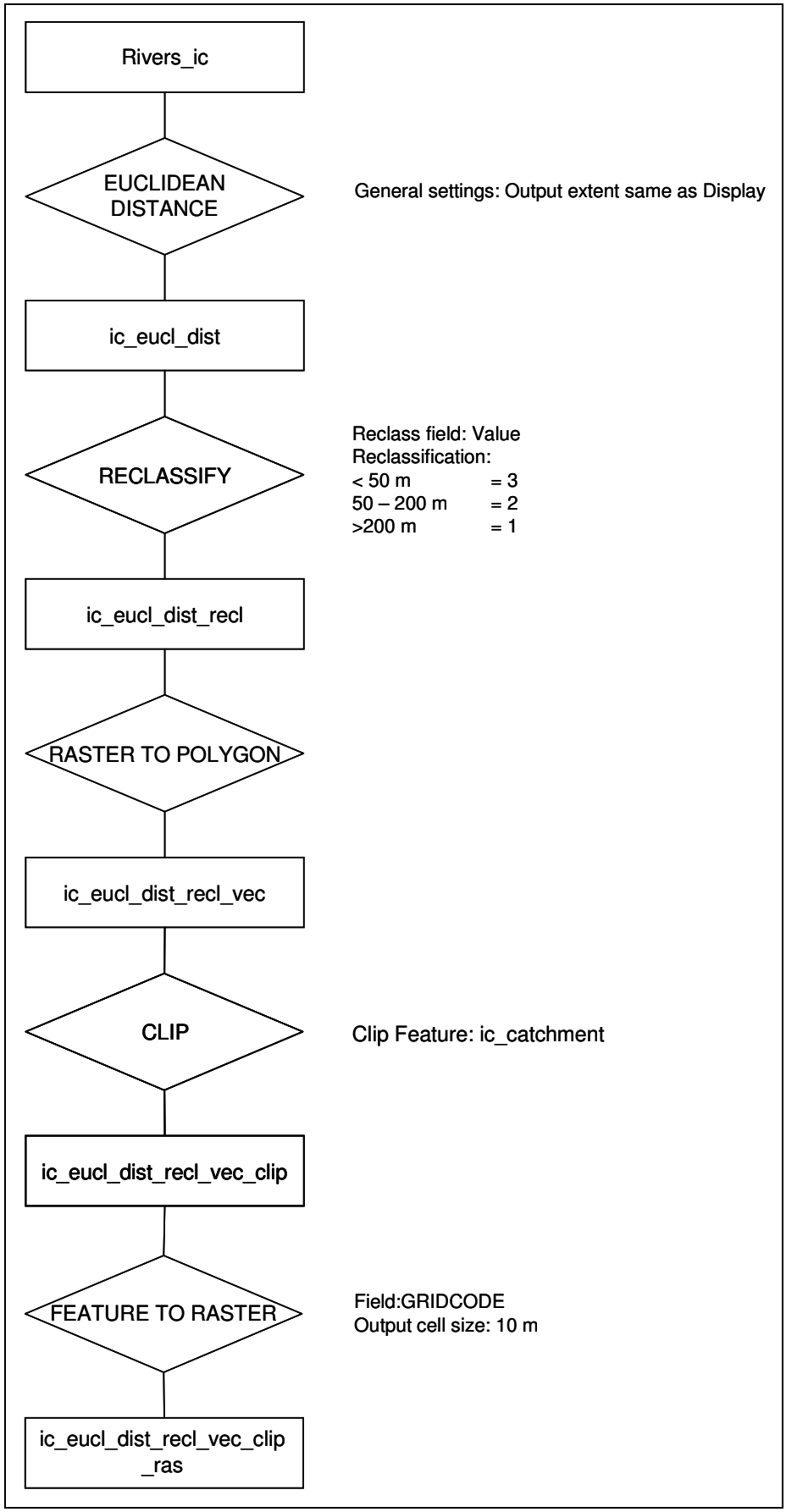

C – Data on the SWAT analysis

C 1. Table of NO_3^- loads predicted by SWAT in 32 subcatchments and according risk classes.

SC	Predicted NO_3 load [kg NO_3^- N ha^{-1} yr^{-1}]	mean RC
1	75.35	2.00
2	58.89	2.13
3	79.45	2.04
4	82.24	1.85
5	28.35	1.52
6	58.77	1.88
7	54.36	2.00
8	77.42	1.84
9	59.99	1.87
10	75.50	1.81
11	67.78	2.03
12	70.02	1.97
13	73.92	1.98
14	80.63	2.17
15	69.86	1.78
16	72.25	1.81
17	86.88	1.90
18	82.08	2.04
19	77.93	1.89
20	95.73	2.17
21	88.88	1.84
22	69.72	1.77
23	71.15	1.82
24	76.00	1.96
25	80.35	2.09
26	79.04	1.99
27	87.19	2.17
28	75.46	1.99
29	85.75	1.99
30	79.77	1.97
31	83.30	2.15
32	8.82	1.63